BES Analysis Memo

ψ' decays to Baryon Pairs

Lingjun Pan
University of Hawaii
Jim Panetta
California Institute of Technology
Stephen L. Olsen
University of Hawaii

Abstract

A sample of 3.4M ψ' decays registered in the BES detector are used to study final states containing pairs of octet and decuplet baryons. We report preliminary branching ratio values for:

		Decay Mode	Branching fraction
ψ'	$\rightarrow$	$p\overline{p}$	$(2.73 \pm 0.21 \pm 0.33) \times 10^{-4}$
	$\rightarrow$	$\Lambda\overline{\Lambda}$	$(2.11 \pm 0.23 \pm 0.26) \times 10^{-4}$
	$\rightarrow$	$\Sigma^0\overline{\Sigma}^0$	$(0.94 \pm 0.30 \pm 0.38) \times 10^{-4}$
	$\rightarrow$	$\Xi^-\overline{\Xi}^+$	$(0.83 \pm 0.28 \pm 0.12) \times 10^{-4}$
	$\rightarrow$	$\Delta^{++}\overline{\Delta}^{--}$	$(0.89 \pm 0.10 \pm 0.24) \times 10^{-4}$
	$\rightarrow$	$\Sigma^-(1385)\overline{\Sigma}^+(1385)$	$(0.56 \pm 0.25 \pm 0.10) \times 10^{-4}$
	$\rightarrow$	$\Xi^0(1530)\overline{\Xi}^0(1530)$	$< 0.75 \times 10^{-4}$
	$\rightarrow$	$\Omega^-\overline{\Omega}^+$	$< 0.83 \times 10^{-4}$

These results are compared to expectations based on flavor-$SU(3)$ symmetry.

1 Introduction

In the quarkonium model, the ψ' is the first radial excitation of the ^3S $c\overline{c}$ bound state. As such, its properties are expected to be relatively straight-forward to understand, at least in terms of those of the J/ψ ground state. Somewhat surprisingly, these expectations do not always hold. In particular, there are two rather dramatic anomalies associated with the ψ':

1. The $\rho\pi$-puzzle. One major puzzle in hadronic ψ decays is the large discrepancy between the decay widths for $J/\psi(1s) \to \rho\pi$ and K^*K and the corresponding widths for $\psi(2s)$ decays. These modes are expected to proceed via $\psi \to ggg$, with widths that are proportional to the square of the $c\overline{c}$ wave function at the origin, which is well determined from dilepton decays. The prediction, known as *"the 14% rule,"* is

$$\frac{Br(\psi' \to X_{had})}{Br(J/\psi \to X_{had})} = \frac{Br(\psi' \to e^+e^-)}{Br(J/\psi \to e^+e^-)} = 0.147 \pm 0.023,$$

where X_{had} designates any exclusive hadronic decay channel. Experimentally, the $\psi(2s) \to \rho\pi$ and K^*K are reduced by over a factor of twenty from these naive expectations [1].

2. The ψ' anomaly. The CDF group has reported a large anomaly in the charmonium production rate in high energy $\overline{p}p$ collisions [2]. It is expected that the J/ψs are mainly decay products of χ states, which are expected to be copiously produced by gluon-gluon fusion. This channel is not expected to be available for ψ' production, and these are expected to be primarily produced via B meson decays. Experimentally, the J/ψ production rate is a factor of two or three above expectations, while that for ψ's exceeds expectations by as much as a factor of thirty.

These anomalies call into question the underlying assumption behind the theoretical predictions, namely that the ψ' is a pure $c\overline{c}$ state.

1.1 $\psi' \to B_8\overline{B_8}$

In the context of flavor $SU(3)$, a pure $c\overline{c}$ state is a flavor singlet and, in the limit of $SU(3)$ flavour symmetry, the phase-space-corrected reduced branching ratios to any baryon octet pair, $|M_i|^2$, where

$$|M_i|^2 = \frac{Br(\psi' \to B_i\overline{B_i})}{\pi p^*/\sqrt{s}}$$

Topology of the octet pairs

Channel	Decay mode	Fraction	Topology
$p\overline{p}$		1.0	$p\overline{p}$
$\Lambda\overline{\Lambda}$	$\Lambda \to p\pi^-$	0.41	$p\overline{p}\pi^+\pi^-$
$\Sigma^0\overline{\Sigma}^0$	$\Sigma^0 \to \Lambda\gamma, \Lambda \to p\pi^-$	0.41	$p\overline{p}\pi^+\pi^-\gamma\gamma$
$\Xi^-\overline{\Xi}^+$	$\Xi^- \to \Lambda\pi^+, \Lambda \to p\pi^-$	0.41	$p\overline{p}\pi^+\pi^-\pi^+\pi^-$

(p^* is the momentum of the baryon in the ψ' rest frame), should be the same for every octet baryon, B_i. Deviations from this rule would indicate a non-$c\overline{c}$ component of the charmonium wave function. The reduced branching fractions for $J/\psi \to B_8\overline{B_8}$ decays are shown in Fig. 1. The $SU(3)$ relation works reasonably well, although there may be some preference for the $p\overline{p}$ mode.

This relation has not been tested for the ψ', where the only relevant branching ratio that has been measured is $\psi' \to p\overline{p}$, and that with rather poor precision [3],[4].

The column "fraction" gives the percentage of the initial state decaying to the indicated final states

1.2 $\psi' \to B_{10}\overline{B}_{10}$

Similarly, we want to make same comparison for ψ' to decuplet pairs with J/ψ as the same as for the octet baryons: $\Delta^{++}\overline{\Delta}^{--}$, $\Sigma^+(1385)\overline{\Sigma}^-(1385)$ + c.c., $\Xi^0(1530)\overline{\Xi}^0(1530)$, and $\Omega^-\overline{\Omega}^+$. The reduced branching fractions for J/ψ to the decuplet baryons are shown in Fig. 2, the data are from PDG tables. From this figure there is a good agreement with the J/ψ being a pure SU(3)-flavor singlet. Also there is no isospin violation in $\Sigma^+\overline{\Sigma}^-$ and $\Sigma^-\overline{\Sigma}^+$ cases. Those are all SU(3) symmetry allowed decays and measured in this paper, the topology of those events is shown in the following tables.

The column "fraction" gives the percentage of the initial state decaying to the indicated final states

2 This experiment

We report preliminary results of measurements of the branching fractions for $\psi' \to B_i\overline{B}_i$, where $B_i = p,\ \Lambda,\ \Sigma^0, \Xi^-, \Delta^{++}, \Sigma^{\pm}(1385), \Xi^-(1530), \Omega^-$ using a sample of 3.4M

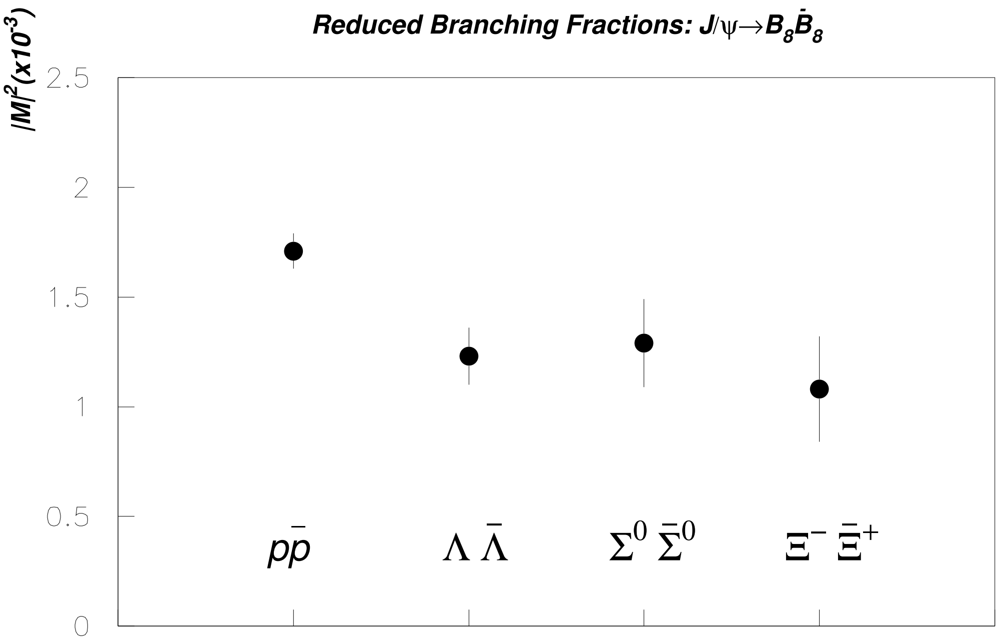

Figure 1: Reduced branching fractions $|M_i|^2$ for $J/\psi(1s) \to B_i\overline{B_i}$, where $B_i = p,\ \Lambda,\ \Sigma^0$, and Ξ^-. The data are from the PDG tables.

Topology of the decuplet pairs

Channel	Decay mode	Fraction	Topology
$\Delta^{++}\overline{\Delta}^{--}$	$\Delta^{++} \to p\pi^+, \overline{\Delta}^{--} \to \overline{p}\pi^-$	> 0.98	$p\overline{p}\pi^+\pi^-$
$\Delta^{++}\overline{p}\pi^-$	$\Delta^{++} \to p\pi^+$	> 0.99	$p\overline{p}\pi^+\pi^-$
$\Sigma^*\overline{\Sigma}^* + \text{c.c.}$	$\Sigma^* \to \Lambda\pi, \Lambda \to p\pi^-$	0.64	$p\overline{p}\pi^+\pi^-\pi^+\pi^-$
$\Xi^0(1530)\overline{\Xi}^0(1530)$	$\Xi^0(1530) \to \Xi^-\pi^+, \Xi^- \to \Lambda\pi^-$	0.41	$p\overline{p}\pi^+\pi^-\pi^+\pi^-\pi^+\pi^-$
$\Omega^-\overline{\Omega}^+$	$\Omega^- \to \Lambda k^-, \Lambda \to p\pi^-$	0.19	$p\overline{p}\pi^+\pi^-k^+k^-$

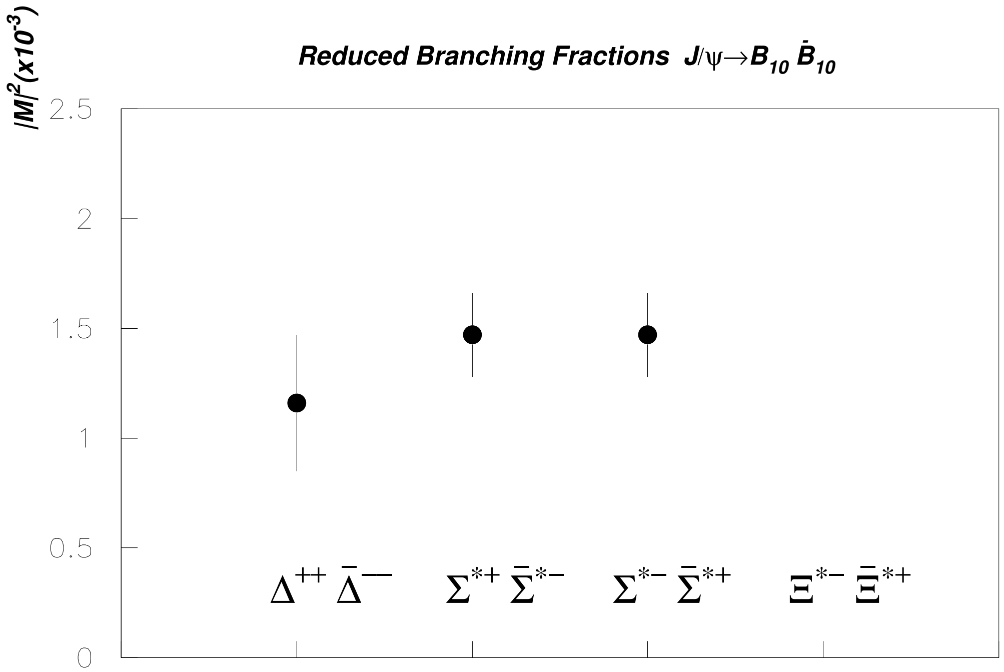

Figure 2: Reduced branching fractions $|M_i|^2$ for $J/\psi(1s) \rightarrow B_i\overline{B}_i$, where $B_i = \Delta^{++}$, Σ^-, and Σ^+. The data are from the PDG tables.

ψ' events produced via e^+e^- annihilations at the BEPC collider and detected in the BES detector.

2.1 The BES detector

The Beijing Electron Spectrometer, BES, is a conventional cylindrical magnetic detector that is coaxial with the BEPC colliding e^+e^- beams. It is described in detail in Ref. [5]. A four-layer central drift chamber (CDC) surrounding the beampipe provides trigger information. Outside the CDC, the forty-layer main drift chamber (MDC) provides tracking and energy-loss (dE/dx) information on charged tracks over 85% of the total solid angle. The momentum resolution is $\sigma_p/p = 0.017\sqrt{1+p^2}$ (p in GeV/c), and the dE/dx resolution for hadron tracks is $\sim 11\%$. An array of 48 scintillation counters surrounding the MDC provides measurements of the time-of-flight (TOF) of charged tracks with a resolution of ~ 450 ps for hadrons. Outside the TOF system, a 12 radiation length, lead-gas barrel shower counter (BSC), operating in self-quenching streamer mode, measures the energies of electrons and photons over $\sim 80\%$ of the total solid angle. The energy resolution is $\sigma_E/E = 0.22/\sqrt{E}$ (E in GeV), and the spatial resolutions are $\sigma_\phi = 4.5$ mrad and $\sigma_z = 4$ cm. Surrounding the BSC is a solenoidal magnet that provides a 0.4 Tesla magnetic field in the central tracking region of the detector. Three double layers of planar counters instrument the magnet flux return (MUID) and are used to identify muons of momentum greater than 0.5 GeV/c. Endcap time-of-flight and shower counters extend coverage to the forward and backward regions.

2.2 The ψ' data samples

The data were accumulated in two runs: a ~ 2.2 pb^{-1} data sample accumulated between December 1993 and January 1994, and a ~ 4.5 pb^{-1} data sample accumulated between December 1994 and March 1995.

3 Event selection

3.1 $\psi' \to p\overline{p}$

The experimental signature for the decay $\psi' \to p\overline{p}$ is two back-to-back, oppositely charged tracks each with three-momentum $p = 1.586$ GeV/c. The positive track, the

Table 1: A tabulation of the momenta for $\psi' \to p\overline{p}$

signal and possible two body backgrounds

	mode	momentum (GeV/c)
signal	p$\overline{p}$	1.586
backgrounds	k^+k^-	1.776
	$\pi^+\pi^-$	1.838
	$\mu^+\mu^-$	1.840
	e^+e^-	1.843

p, typically deposits one-half or less of its 0.91 GeV kinetic energy in the BSC; the negative $\overline{p}$ undergoes an annihilation process in the BSC approximately half the time, producing an energy cluster that can occasionally exceed the beam energy.

Potential two-body backgrounds and their corresponding 3 momenta are in Table 1.

Other backgrounds arise from other two-body decays of the ψ', cosmic rays, and cascade decays of the types $\psi' \to \pi\pi J/\psi$ and $\psi' \to \gamma\chi_c$, where the J/ψ or χ_c decay to a two-body final state and the accompanying particles are not seen in the detector.

3.1.1 $p\overline{p}$ preselection criteria:

We select events with two charged tracks:

1. skip bad runs
2. two, and only two, well reconstructed oppositely charged tracks;
3. have muid1 .ne. 1 .or. muid2 .ne. 1 (i.e. muid code from trklst) to eliminate obvious μ pairs (where both trks have muid =1)
4. have $|\cos\theta|$ <0.8 for both tracks
5. have $|(tof)|$ <50.0 ns for both tracks to eliminate events where the TOF system failed.
6. these events are subject to 4-c fits using Telesis the hypotheses: $\psi' \to k^+k^-$ and $\psi' \to p\overline{p}$ with a
7. $\chi^2_{p\overline{p}} < 50.$ in telesis ($\psi' \to k^+k^-$ is the two body mode with kinematics closest to that of $p\overline{p}$.)

3.1.2 $p\overline{p}$ selection criteria:

We extract a clean sample of $\psi' \to p\overline{p}$ events by imposing the following selection requirements on the recorded event samples:

1. Solid angle cuts.
   Figs. 3a and b show the $\cos\theta$ distributions for the plus and minus tracks. Bhabhas are evident as peaks in the backward (forward) directions for the plus (minus) tracks.
   $|\cos\theta^{+}| <0.6$ .and. $|\cos\theta^{-}| <0.6$
   this restricts us to events that point within the solid-angle acceptance of the muon chambers

2. Time of Flight cuts
   Fig. 3c shows the difference in TOF-determined times for the plus and minus tracks. The small peaks at +/- 8 nanosecs are apparently due to cosmic rays. We eliminate these with a (crude) TOF-difference cut:
   $|T_p - T_{\overline{p}}| <4.0$ ns

3. Shower counter cuts
   Figs. 3d and e show the shower energies for the tracks. The sharp edges at 0.8 reflect the effects of the preselection cut. We attribute the excess of high energy showers in Fig. 3e to $\overline{p}$ annihilations in the BSC. Such large showers are not expected for protons. We suppress e^+e^- pairs remaining in the data with a cut on proton shower energies:
   $E_p < 0.8$ GeV

4. Unmatched gamma energy cuts.
   Fig. 3f shows the sum of the energy of the neutral showers that are more than 30 degrees from either charged track (to avoid counting ghost showers) and have less than 80% of its total energy in a single layer (to avoid counting noise hits). Backgrounds from $\psi' \to \pi^0\pi^0 J/\psi$; J/$\psi \to$ two tracks, and $\psi' \to \gamma\chi$; $\chi \to$ two tracks likely produce such showers. We make the cut:
   $E_{\gamma}^{unmatch} <0.1$ GeV

5. $k^+k^-/p\overline{p}$ chisquare difference cut
   Figs. 4a, b, and c show the distributions of χ^2 to the k^+k^- hypotheses, the $p\overline{p}$ hypotheses, and the scatter plot. Non $p\overline{p}$ two body modes should give better

fits to the k^+k^- hypotheses than to $p\overline{p}$. They show up in Fig. 4c as the peak at negative chisquare difference values. We cut these events:
$\chi^2_{k^+k^-} > \chi^2_{p\overline{p}}$

6. Momentum difference cut.
Fig. 4d shows the difference in pre-fit values of the 3-momentum of the two tracks. Fig. 4e shows the same difference for the events with $\chi^2_{p\overline{p}} > 20$. The poor chisquare events, likely due to two-body decays of cascade J/ψ's and χ-states, tend to have 3-momentum differences that are distinct from zero. We exploit this with the cuts on the pre-fit momentum difference
$|p^+ - p^-|$ <0.2 GeV/c

7. p pbar chisquare cut:
Fig. 4f shows the chisquare for the $p\overline{p}$ hypothesis for the surviving events. There is a clear peak that does not appear to extend much beyond chisquare values of 15, with a tail that extends out to preselect limit of 50. We require
$\chi^2_{p\overline{p}} < 15$.

The $|\cos\theta| \leq 0.6$ requirement restricts the tracks to the solid angle region that is well covered by the MUID system. The MUID requirement eliminates obvious $\psi' \to \mu^+\mu^-$ and continuum $e^+e^- \to \mu^+\mu^-$ events. The loose TOF difference requirement is sufficient to eliminate all cosmic ray events. The limit on the BSC energy associated with the positive track eliminates e^+e^- events while keeping signal events where the $\overline{p}$ annihilates in the BSC. The unmatched BSC energy and momentum difference requirements preferentially eliminate events from cascade decays.

Each event that survives these cuts is subjected to four-constraint kinematic fits to the hypotheses $\psi' \to p\overline{p}$ and $\psi' \to K^+K^-$. We only keep those events that have $\chi^2_{K\overline{K}} > \chi^2_{p\overline{p}}$. (The K^+K^- mode is the two-body mode that is the most kinematically similar to the $p\overline{p}$ mode.) The resulting $\chi^2_{p\overline{p}}$ distribution, shown in Fig. 4f, shows a strong enhancement for low χ^2 values, indicating a $\psi' \to p\overline{p}$ signal.

The events passing the above cuts are shown in Fig. 8a.

The effects of the various selection cuts on the data and the simulated event sample is summarized in Table 2.

The plots for the MC data with angular distribution 1+0.21$\cos^2\theta$ which correspond to the data are shown in Figure 5, Figure 6,Figure 7.

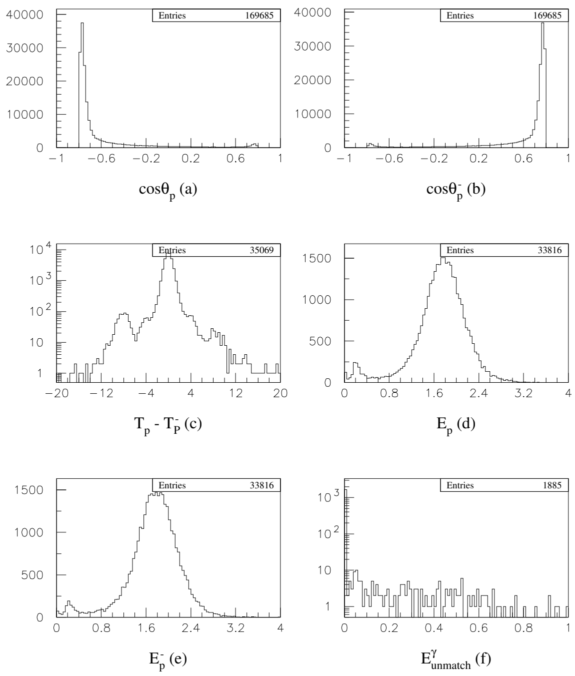

Figure 3: The distributions of selected events that fit $\psi' \to p\overline{p}$ cuts

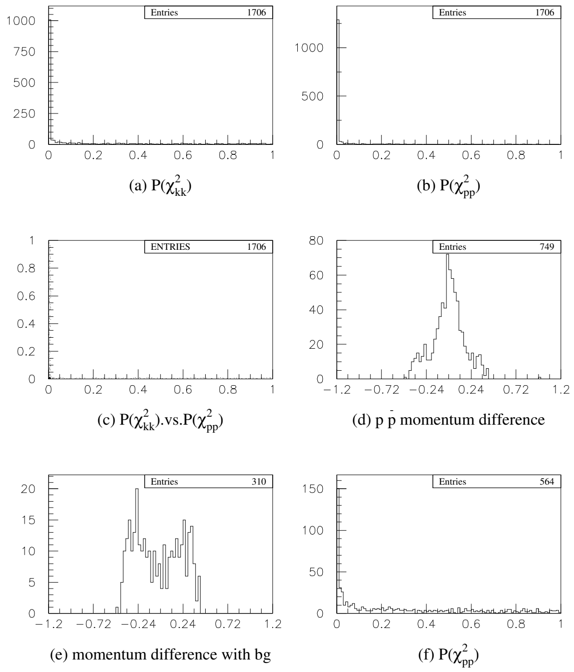

Figure 4: The distributions of selected events that fit $\psi' \to p\overline{p}$ cuts

Table 2: A tabulation of the $\psi' \to p\overline{p}$ selection cuts.

Numbers of events surviving each requirement

	94 data	95 data	Simulated events
Preselection:			
Generated			10000
skip bad runs	1482052	3053390	10000
2 chrgd trks, $\sum q = 0$	888569	1737453	8792
veto $\mu^+\mu^-$	807323	1571768	8792
$\lvert\cos\theta\rvert$ <0.8	601173	1160476	7480
$T_{trk} < 50$ ns	601158	1160318	7327
$\chi^2_{p\overline{p}}$ <50.	63324	106361	7303
$\lvert\cos_{trk}\theta^+\rvert$ <0.6, $\lvert\cos\theta^-\rvert$ <0.6	12061	23008	5297
$\lvert T_p - T_{\overline{p}}\rvert$ <4.0 ns	11699	22117	5297
$E_p < 0.8$ GeV	593	1292	5297
$E_\gamma^{unmatch}$ <0.1 GeV	506	1200	5297
$P(\chi^2_{kk}) < P(\chi^2_{pp})$	242	507	5273
$\lvert p^+ - p^-\rvert < 0.2$ GeV/c	188	376	5226
$P(\chi^2_{p\overline{p}})$ <1%	143	271	5004

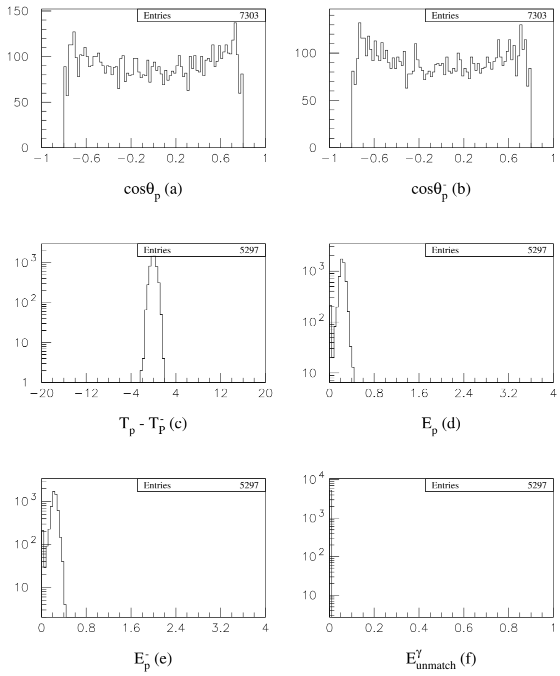

Figure 5: The distributions of selected events that fit $\psi' \to p\overline{p}$ cuts

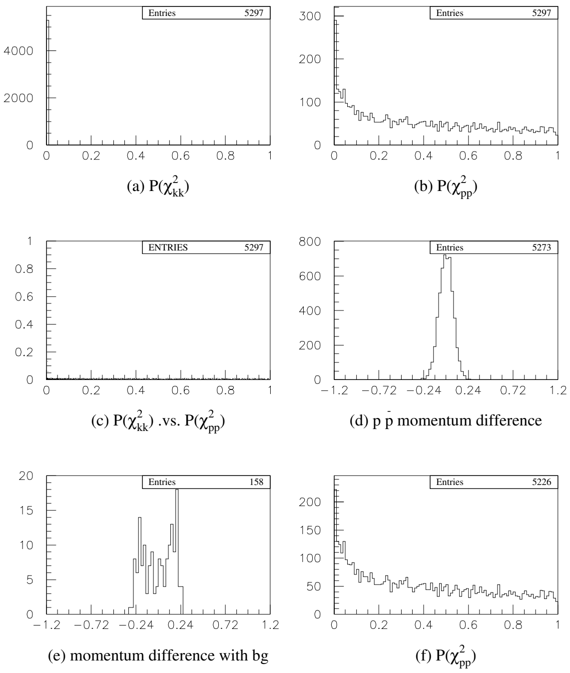

Figure 6: The distributions of selected events that fit $\psi' \to p\overline{p}$ cuts

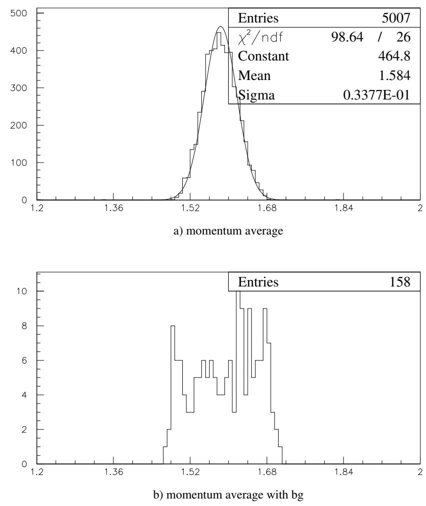

Figure 7: The average momentum for selected MC events that fit $\psi' \to p\overline{p}$ with: **a)** $\chi^2 \leq 15$; **b)** $\chi^2 \geq 20$.

3.1.3 $p\overline{p}$ signal:

Figure 8a shows the average momentum of the two tracks for events with $\chi^2_{p\overline{p}} \leq 15$. There is a clear peak with 320 events that is well fit by a gaussian with a peak at $p_{avg} = 1.591 \pm 0.003$ GeV/c and an rms width of $\sigma = 3.8 \pm 0.3$ MeV/c, shown in Fig. 8, consistent with expectations for $\psi' \to p\overline{p}$ and the BES momentum resolution.

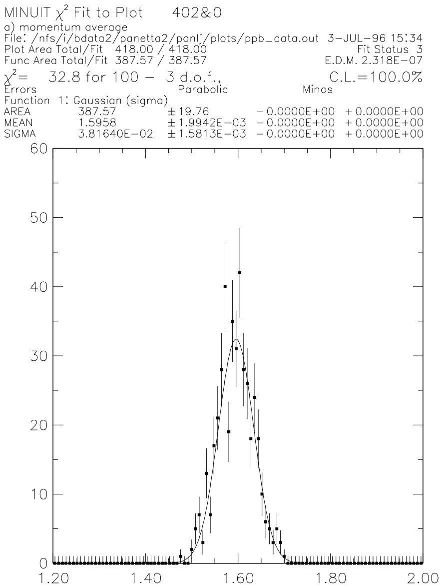

Figure 8: The average momentum for selected events that fit $\psi' \to p\overline{p}$ with: $P(\chi^2) > 0.01$

3.1.4 $p\overline{p}$ residual background:

There is no evidence for residual backgrounds from two-body decays in Fig. 9. Contamination from $\psi' \to K^+K^-$ decays are expected to have average momentum values centered near $p_{avg} = 1.776$ GeV/c, where no events are seen. Figure 9 shows the average momentum of selected events with $\chi^2_{p\overline{p}} \geq 20$. This distribution has a peak near $p_{avg} \simeq 1.65$ GeV/c, which is where backgrounds from the cascade decays $\psi' \to \gamma\chi_{c_0}(3410)$ followed by the two-body decay $\chi_{c_0}(3410) \to \pi^+\pi^-$ are expected. In addition there are a few events with average momentum values below that expected for $\psi' \to p\overline{p}$ decays. These are kinematically consistent with cascade decays $\psi' \to \pi\pi J/\psi$, where neither π is seen in the detector and the J/ψ subsequently decays to charged particle pairs.

Monte Carlo simulations of both of the above-mentioned cascade processes indicate that they tend to have high values of $\chi^2_{p\overline{p}}$; less than 20% of the simulated cascade events that are selected with $\chi^2_{p\overline{p}} \leq 50$ have $\chi^2_{p\overline{p}} \leq 15$. We estimate the background in the selected $p\overline{p}$ event sample by attributing all of the events with $\chi^2_{p\overline{p}} \geq 20$ in Fig. 8b to these sources and use the Monte Carlo results to extrapolate to lower $\chi^2_{p\overline{p}}$ values. The resulting background estimate is $N_{bkg} = 33 \pm 33$ events, where we have conservatively assigned a 100% error.

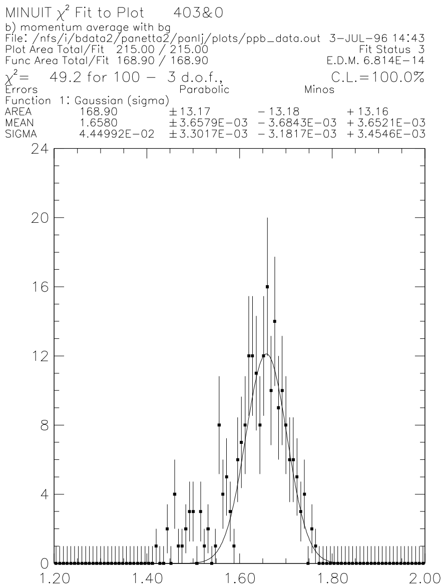

Figure 9: The average momentum for selected events that fit $\psi' \rightarrow p\overline{p}$ with: $P(\chi^2) < 0.01$

3.2 $\psi' \rightarrow \Lambda\overline{\Lambda}$

The decays $\psi' \rightarrow \Lambda\overline{\Lambda}$ produce two back-to-back Λ's, each with three-momentum $p = 1.467$ GeV/c. We only consider events where both Λ's decay to charged $p\pi$ final states. The final states of interest are, thus, $\psi' \rightarrow \pi^+\pi^-p\overline{p}$, where the π^-p and $\pi^+\overline{p}$ originate from well separated decay vertices with a mean decay length of 10.4 cm.
$(c\tau \times \frac{q_{avg}}{M_\Lambda} = 7.89 \times \frac{1.467}{1.116} = 10.4\ cm.)$
The decay kinematics of the Λ's are such that the proton (antiproton) is always the highest momentum positive (negative) track in the event, according to Table 3.

3.2.1 $\Lambda\overline{\Lambda}$ selection criteria:

We extract $\psi' \rightarrow \Lambda\overline{\Lambda}$ event candidates using the following selection criteria:

Table 3: A tabulation of the momenta of p and π from $\psi' \to \Lambda\overline{\Lambda}$

Momenta of p and π in GeV/c

	p	π
max momentum	1.41	1.39
min momentum	1.08	0.06

1. skip bad runs
2. four, and only four, well reconstructed charged tracks with a zero net charge;
3. all four tracks are in the polar angle region $|\cos\theta| \leq 0.8$;
4. $E_1 \leq 0.8$ OR $E_2 \leq 0.8$ GeV, where E_1 (E_2) is the BSC energy deposit associated with the highest momentum positive (negative) track; and
5. Either the highest-momentum positive or negative track is not positively identified by the MUID as a muon.
6. Passing KLAMSLOW
   Events where tracks 1($\overline{p}$) and 4(π^+) and tracks 2(p) and 3 (π^-) are successfully verticized by KLAMSLOW.
7. Events are subjected to a 5-C fits to hypothesis state $p\overline{p}\pi^+\pi^-$, and Telesis returns events that:
   $\chi^2_{p\overline{p}\pi^+\pi^-} < 50$.

The polar angle requirement restricts tracks to the solid angle region that is well covered by the MDC. The BSC (MUID) requirement eliminates cascade events of the type $\psi' \to \pi^+\pi^- J/\psi$; followed by $J/\psi \to e^+e^-$ ($\mu^+\mu^-$).

Both πp pairs in the surviving events are processed through a displaced vertex-finding algorithm and the event is then subjected to a five-constraint kinematic fit to the hypothesis $\psi' \to \pi^+\pi^- p\overline{p}$, including a "beam constraint:" $M_{\pi^- p} = M_{\pi^+\overline{p}}$. Here the highest momentum positive (negative) track is classified as the proton (antiproton).

Further selection cuts are made to select more clear Λ signals.

1. $\chi^2_{p\overline{p}\pi^+\pi^-} < 15$.
   Fig. 10a shows the fitted pπ^- mass distribution for the events that survive the

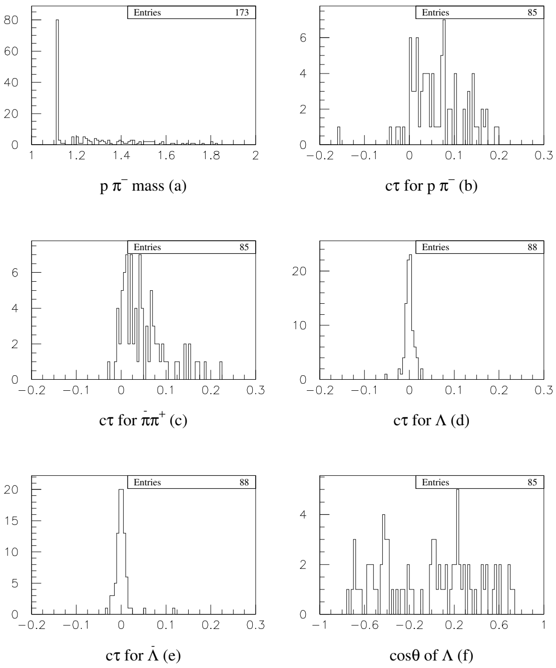

Figure 10: Distributions for selecting the events for $\psi' \to \Lambda\overline{\Lambda}$

cuts. A sharp peak at the Lambda mass with little (no?) background is apparent. We select Lambda events by requiring

2. $M_{p\pi^-}$ <1.15 GeV
(The 5th constraint forces $M_{\overline{p}\pi^+} = M_{p\pi^-}$.) Figs. 10b and Figs. 10c show the ctau values output by KLAMSLOW for the 1, 4 ($\overline{p}\pi^+$) and 2, 3 (p π^-) combinations with mass in the Lambda peak (M<1.15 GeV), respectively. Figs. 10d and 10e show the ctau distributions for the same track combinations with masses outside the Λ region (M>1.15 GeV).

The effects of the various selection cuts on the data and the simulated event sample is summarized in Table 4.

The ctau distribution for π^-p combinations have a broad dsitribution, consistent with the 7.89 cm lifetime of the Λ. We scanned the events with large negative $c\tau$ values, and these were all "sailor' type events with two possible crossing points where, apparently, KLAMSLOW selected the wrong one. Figure 11 shows a zoomed view of event 7718/7268. KLAMSLOW returns a value of $c\tau$ = -0.054 m for tracks 1 and 2, where a crossing with a positive $c\tau$ value is also obvious.

Fig.. 10f shows the $\cos\theta$ distribution of the selected events in the Λ mass peak.

Similar plots for the MC data with angular distribution $1+0.67cos^2\theta$ are shown in Figure 12, and Λ angular distribution for generated MC events is shown in Figure 13.

3.2.2 $\Lambda\overline{\Lambda}$ signal:

The distribution of fitted πp invariant masses for events with $\chi^2 \leq 15$, shown in Fig. 10, has a clear peak at the $M = 1.116$ GeV mass of the Λ.

The $c\tau$ values for events in the Λ peak are consistent with the PDG value of $c\tau_\Lambda =$ 7.89 cm; those for the events outside of the peak are consistent with $c\tau = 0$.

3.2.3 $\Lambda\overline{\Lambda}$ residual background:

There is no evidence for any significant background either in the πp mass plot or the $c\tau$ distributions. If, in Fig. 10, we assume a flat background and extrapolate under the Λ mass peak we find five "background" events in the Λ sample. We conservatively assign a 100% error to this background estimate and use $N_{bkg} = 5 \pm 5$ in the branching fraction calculation.

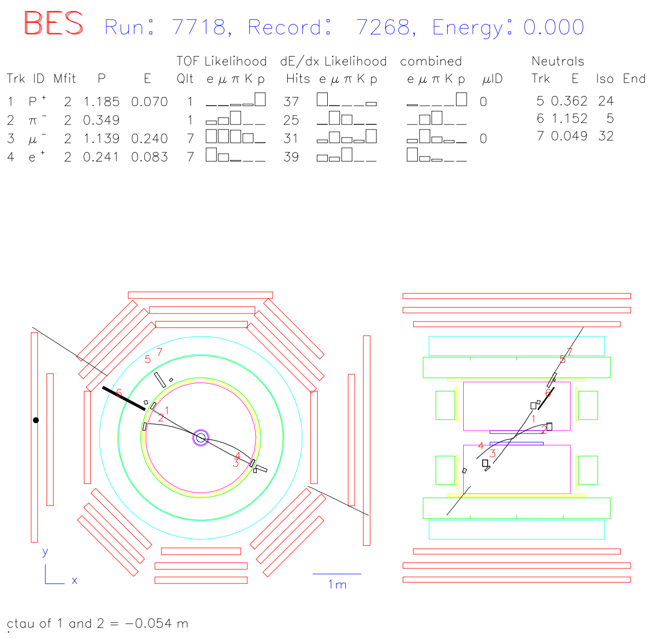

Figure 11: Event display for $\psi' \rightarrow \Lambda\overline{\Lambda}$

Table 4: A tabulation of the $\Lambda\overline{\Lambda}$ selection cuts.

Numbers of events surviving each requirement

	94 data	95 data	Simulated events
Preselection:	769831	1554221	
Generated			10000
skip bad runs	761640	1545198	10000
4 chrgd trks and $\sum$ q=0	317504	597451	6164
veto $\mu^+\mu^-$	303980	570412	6164
$\lvert \cos\theta_{chg} \rvert \leq 0.8$	187038	345289	4859
passing klamslow	142946	262032	3770
$\chi^2_{p\overline{p}\pi^+\pi^-} < 50.$	158	276	3214
Selection:			
P($\chi^2_{p\overline{p}\pi^+\pi^-}$) < 1%	67	106	2766
$M_{p\pi^-}$ <1.15 GeV	28	57	2766

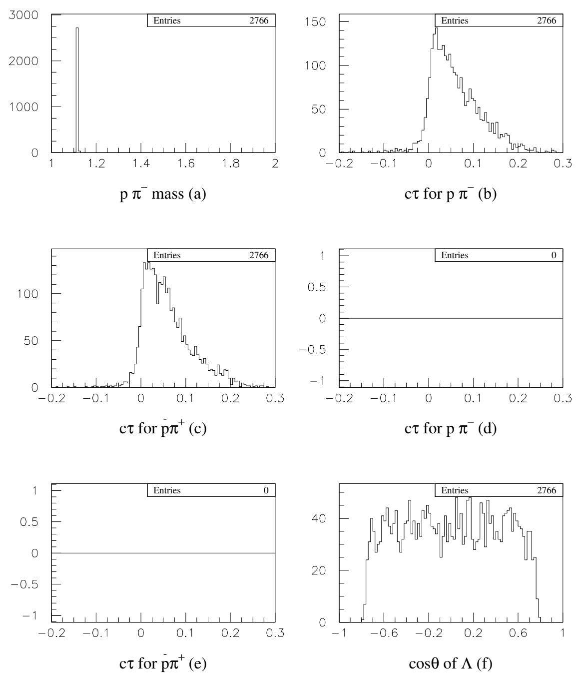

Figure 12: Event selection for MC data for $\psi' \to \Lambda\overline{\Lambda}$

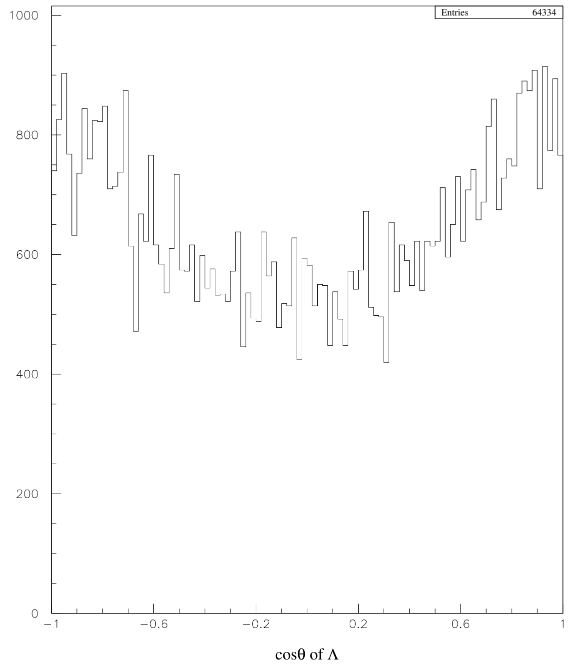

Figure 13: Angular distribution for MC data for $\psi' \to \Lambda\overline{\Lambda}$

Table 5: A tabulation of the momenta of Σ^0 production in GeV/c

Momentum ranges of Σ^0 decaying production

	γ	Λ	p	π
max momentum	0.201	1.431	1.373	0.386
min momentum	0.0	1.202	0.867	0.037

3.3 $\psi' \to \Sigma^0\overline{\Sigma}^0$

The Σ^0 hyperons from $\psi' \to \Sigma^0\overline{\Sigma}^0$ decay promptly via $\Sigma^0 \to \gamma\Lambda$. We consider only those decays where the Λ's decay via the charged πp modes. The experimental signature is, thus, $\psi' \to \pi^+\pi^-p\overline{p}\gamma\gamma$, where the π^-p and $\pi^+\overline{p}$ originate from Λ hyperons with well separated decay vertices with a mean decay length of 9.2 cm.
$(c\tau \times \frac{q_{avg}}{M_\Lambda} = 7.89 \times \frac{1.3}{1.116} = 9.2\ cm.)$
In addition, there are two γ rays in the energy range $0 \leq E_\gamma \leq 201$ MeV. As in the case for $\psi' \to \Lambda\overline{\Lambda}$, the proton (antiproton) is always the highest momentum positive (negative) track in the final state, according to the kinematic calculations in Table 5.

3.3.1 $\Sigma^0\overline{\Sigma^0}$ selection criteria:

We extract $\psi' \to \Sigma^0\overline{\Sigma}^0$ event candidates through $\Sigma^0 \to \Lambda\gamma$, $\overline{\Sigma}^0 \to \overline{\Lambda}\gamma$, and $\Lambda \to p\pi^-$, $\overline{\Lambda} \to \overline{p}\pi^+$ using the same selection criteria as used for the $\Lambda\overline{\Lambda}$ mode with the additional requirement:

- two or more isolated BSC clusters with $E_{BSC} > 50$ MeV and within the polar angle region $|\cos\theta| \leq 0.8$.

By *"isolated"* we mean more than 30^0 away from each of the charged tracks.

Both πp pairs in the surviving events are processed through a displaced vertex-finding algorithm and the event is then subjected to five-constraint kinematic fits to the hypothesis $\psi' \to \pi^+\pi^-p\overline{p}\gamma\gamma$, including the beam constraint $M_{\pi^-p\gamma} = M_{\pi^+\overline{p}\gamma}$. Here the highest momentum positive (negative) track is classified as the proton (antiproton). For events with more than two γ candidates, the fit is applied for each combination of two. For each two-γ combination, fits are tried with each γ associated, in turn, with each πp pair. The combination with the best χ^2 value is selected.

Further selection cuts are made as follows:

1. The χ^2 distribution for the all data is shown in Fig 14a. We cut off the χ^2 as following:
   $\chi^2_{p\overline{p}\pi^+\pi^-\gamma\gamma} < 15.$
   Fig. 14b shows the fitted $p\pi^-\gamma$ mass distribution for the events that survive the χ^2 cut. A small but distinct peak at the Σ^0 mass is apparent. We make a loose cut of $\pm$ 30 MeV around the Σ^0 mass and examine these events. (This is not one of our final selection cuts.)

2. Figure 14c,d shows the $p\pi^-$ ($\overline{p}\pi^+$) mass distribution for these events. The clear Λ ($\overline{\Lambda}$) peak is apparent. We select events within $\pm$ 20 MeV of the Λ ($\overline{\Lambda}$) mass, i.e.
   $1.095 < M_{p\pi^-} < 1.135\ GeV.$
   $1.095 < M_{\overline{p}\pi^+} < 1.135\ GeV.$

Figs. 14e and f show the $c\tau$ values output by KLAMSLOW for the 1, 4 ($\overline{p}\pi^+$) and 2, 3 ($p\pi^-$) combinations, respectively.

The effects of the various selection cuts on the data and the simulated event sample is summarized in Table 6.

3.3.2 $\Sigma^0\overline{\Sigma}^0$ signal:

Figure 15 shows the $\pi p\gamma$ invariant masses for the events with $\chi^2 < 15$ where both πp invariant masses are within ± 20 MeV of M_Λ. A peak at $M_{\Sigma^0} = 1.193$ GeV is evident. We fit this spectrum to a single gaussian and a flat background. The fit gives a background-subtracted signal of 10.9 ± 3.7 events in a peak centered at $M_{\pi p\gamma} = 1.190 \pm 0.003$ GeV, consistent with M_{Σ^0}.

3.3.3 $\Sigma^0\overline{\Sigma}^0$ background:

There is no evidence for any significant backgrounds in the pπ^- mass plot or in the cτ distributions. If in Fig. 15, we assume a flat background, an extrapolation under the Λ mass peak gives a background of 3 events or 6%. We take 3 $\pm$ 3 as an estimate of the background.

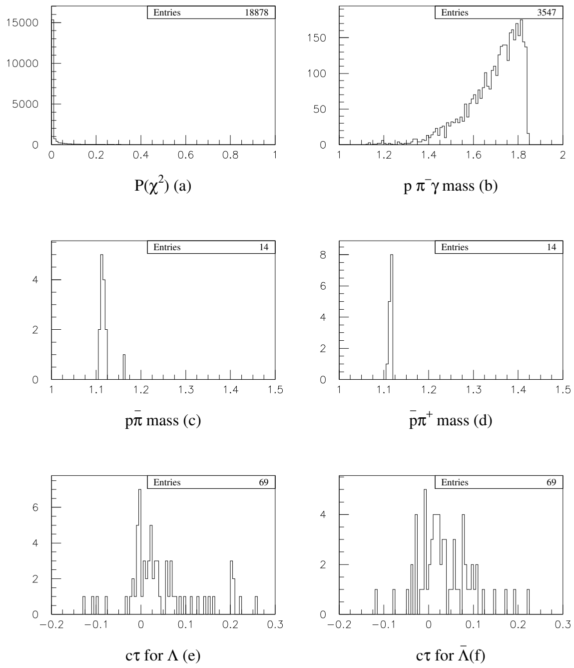

Figure 14: Distributions for selecting event for $\psi' \to \Sigma^0\overline{\Sigma}^0$

Table 6: A tabulation of the $\Sigma^0\overline{\Sigma^0}$ selection cuts.

Numbers of events surviving each requirement

	94 data	95 data	Simulated events
Preselection:			
Generated			10000
skip bad runs	761640	1545198	10000
4 chrgd trks, $\sum q = 0$	265033	487139	3368
veto $\mu^+\mu^-$	260322	476460	3368
$\lvert\cos\theta_{chg}\rvert \leq 0.8$	163134	296389	2577
passing klamslow	97280	225099	2045
$\chi^2_{p\overline{p}\pi^+\pi^-} < 50.$	7552	13251	1330
$E_\gamma > 0.05$ GeV	6847	12031	884
$P(\chi^2_{p\overline{p}\pi^+\pi^-}) < 1\%$	1297	2250	752
$1.095 < M_{p\pi^-} < 1.135$, $1.095 < M_{\overline{p}\pi^+} < 1.135$ GeV	22	47	734

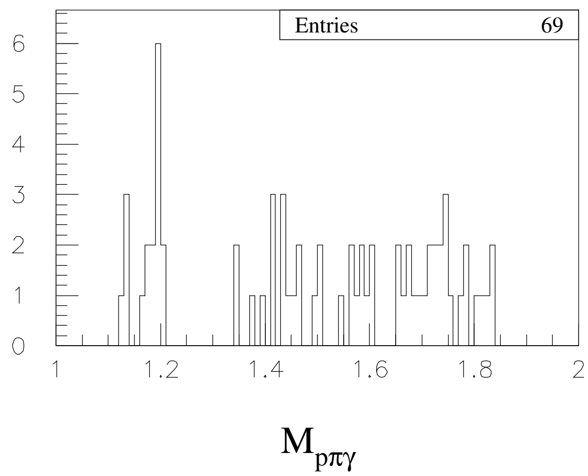

Figure 15: The $M_{\pi p\gamma}$ distribution for events with $\chi^2 < 15$ and where both πp masses are within ± 20 MeV of M_Λ.

Table 7: A tabulation of the momenta of Ξ production in GeV/c

Momentum ranges for Ξ decaying production

	orphan π	Λ	p	decaying π
max momentum	0.385	1.287	1.243	0.353
min momentum	0.0	0.899	0.629	0.009

3.4 $\psi' \to \Xi^-\overline{\Xi}^+$

The Ξ^- hyperon from $\psi' \to \Xi^-\overline{\Xi}^+$ decays via $\Xi^- \to \pi^-\Lambda$ and $\overline{\Xi}^+ \to \pi^+\overline{\Lambda}$. We consider only those decays where the Λ's decay via the charged πp modes. The experimental signature is $\psi' \to \pi^+\pi^-\pi^+\pi^- p\overline{p}$ where one each of the $\pi^- p$ and $\pi^+\overline{p}$ combinations originate from Λ hyperons with average momentum = 1.1 GeV/c and have well separated decay vertices with a mean decay length L of
$c\tau \times \frac{q_{avg}}{M_\Lambda} = 7.89 \times \frac{1.1}{1.116} = 7.8\ cm$.
As in the case for $\psi' \to \Lambda\overline{\Lambda}$ and $\Sigma^0\overline{\Sigma}^0$, the proton (antiproton) is always the highest momentum positive (negative) track in the final state, as shown in the following Table 7.

3.4.1 $\Xi^-\overline{\Xi}^+$ selection criteria:

We extract $\psi' \to \Xi^-\overline{\Xi}^+$ event candidates using the following selection criteria:

1. six, and only six, well reconstructed charged tracks with a zero net charge and all in the polar angle region $|\cos\theta| \leq 0.8$;

2. $E_1 \leq 0.8$ OR $E_2 \leq 0.8$ GeV, where E_1 (E_2) is the BSC energy deposit associated with the highest momentum positive (negative) track; and

3. either the highest-momentum positive or negative tracks are not positively identified by the MUID as a muon.

The motivation for these criteria are the same as for the case of $\Lambda\overline{\Lambda}$, discussed above.

We loop over each event four times, processing each possible $\pi^- p$ and $\pi^+\overline{p}$ combination through a displaced vertex-finding algorithm and then subjecting the event to a five-constraint kinematic fit to the hypothesis $\psi' \to \pi^+\pi^-\pi^+\pi^- p\overline{p}$, with the beam constraint $M_{\pi^-\pi^-p} = M_{\pi^+\pi^+\overline{p}}$. Here the highest momentum positive (negative) track is identified as the proton (antiproton).

The combination with the best χ^2 value is selected. Telesis returns events with $\chi^2 < 50$.

Further cuts are made to select Ξ signals.

1. The χ^2 distribution for all data is shown in Fig. 16a. The fitted p pi- pi- mass distribution for all events, shown in Fig. 16b, has a clear peak at the Ξ^- mass (1.321 GeV). No further cuts are needed to isolate a $\Xi^-\overline{\Xi}^+$ signal.
   $\chi^2_{p\overline{p}\pi^+\pi^-\pi^+\pi^-}(5-C) < 15$.

2. The number of $\Xi^-\overline{\Xi}^+$ events is taken to be the number of events within $\pm$ 30 MeV of the Ξ mass.
   $1.291 < M_{\Xi} < 1.351$ GeV

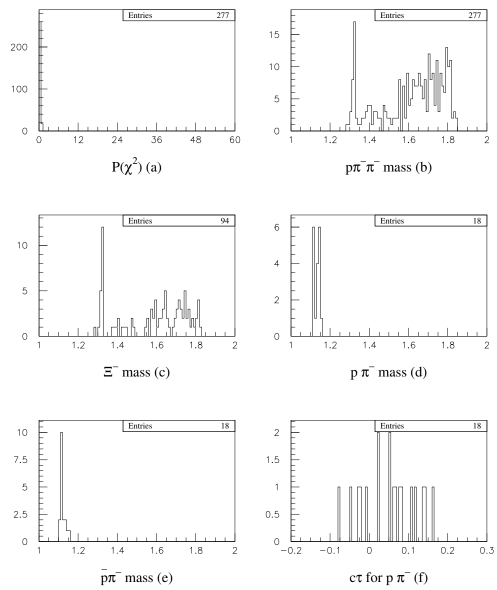

Figure 16: The distributions for events that pass the cuts for $\psi' \to \Xi^-\overline{\Xi}^+$

3.4.2 $\Xi^-\overline{\Xi}^+$ signal:

The distribution of fitted invariant $\pi\pi p$ masses for events with $\chi^2 \leq 15$, shown in Fig. 17, has a clear and distinct peak at the $M = 1.321$ GeV Ξ^- mass. We select the

Table 8: A tabulation of the $\Xi^-\overline{\Xi}^+$ selection cuts.

Numbers of events surviving each requirement

	94 data	95 data	Simulated events
Preselection:	655502	1238869	
Generated			10000
skip bad runs	649193	1232381	10000
6 chrgd trks, $\sum q = 0$	335918	625466	3471
veto $\mu^+\mu^-$	331662	614255	3471
$\lvert\cos\theta_{chg}\rvert \leq 0.8$	173575	318183	2307
$\chi^2_{p\overline{p}\pi^+\pi^-} < 50.$	91	186	1504
$P(\chi^2_{p\overline{p}\pi^+\pi^-}) < 1\%$	39	55	1500
$\lvert M_{p\pi^-\pi^-} - M_{\Xi}\rvert$ <0.03 GeV	7	11	1142

events within ±30 MeV of the Ξ^- mass as $\psi' \to \Xi^-\overline{\Xi}^+$ event candidates; no further cuts are made.

3.4.3 $\Xi^-\overline{\Xi}^+$ residual background:

To estimate the residual background in the sample of $\Xi^-\overline{\Xi^-}$ event candidates, we repeat the fit procedure with the wrong-sign hypothesis $\Xi^- \to \pi^+\Lambda$, etc., and requiring $M_{\pi^+\pi^-p} = M_{\pi^-\pi^+\overline{p}}$. We normalize the $M_{\pi^+\pi^-p}$ distribution for $\chi^2 \leq 15$ events to that for the right-sign sample using the number of events outside of the M_{Ξ^-} mass region. We determine the number of background events to be $N_{bkg} = 1.4 \pm 1.4$ events, shown in Fig. 18.

4 Event Selection for ψ' to the Decuplet Baryon Pairs

4.1 $\psi' \to \Delta^{++}\overline{\Delta}^{--}$

The decays $\psi' \to \Delta^{++}\overline{\Delta}^{--}$ produce two back-to-back Δ^{++} and $\overline{\Delta}^{--}$ with 3-momentum P = 1.371 GeV. We select events where both Δ^{++} and $\overline{\Delta}^{--}$ decay to p pi [Br($\Delta^{++} \to p\pi$) > 99 %]. The final states are $\psi' \to p\pi^+\overline{p}\pi^-$. The decay kinematics of the Δ^{++} and

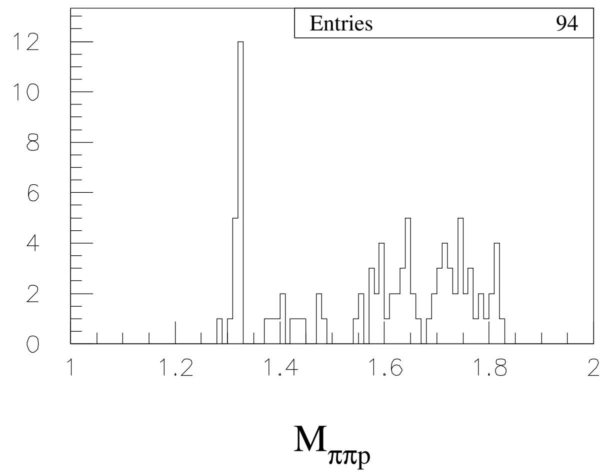

Figure 17: The fitted $M_{\pi\pi p}$ distribution for events with a best-fit $\chi^2 \leq 15$ to a five-constraint fit to $\psi' \to \pi^+\pi^-\pi^+\pi^- p\overline{p}$; $M_{\pi^-\pi^-p} = M_{\pi^+\pi^+\overline{p}}$.

$\overline{\Delta}^{--}$ are such that the proton (antiproton) are always the highest momentum positive (negative) track in the event, as shown in the Table 9.

4.1.1 Event Selection Criteria

We extract $\psi' \to \Delta^{++}\overline{\Delta}^{--}$ event candidates using the following selections:

1. four, and only four, well reconstructed charged tracks with a zero net charge;

Table 9: A tabulation of the momenta of Δ production

Momenta of p and π in Δ^{++} production in GeV/c

	p	π
max momentum	1.417	0.638
min momentum	0.736	0.0

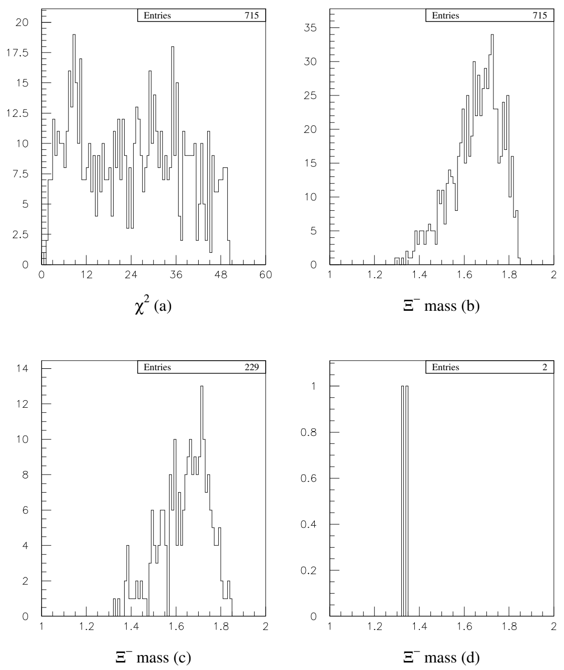

Figure 18: The fitted $M_{\pi\pi p}$ distribution for the wrong sign orphan pions in the beam constraint

2. all four tracks are in the polar angle region $|\cos\theta| \leq 0.8$, and mfit = 2, or -9, or -19;

3. either the highest-momentum positive or negative track is not positively identified as a muon by μ selection cuts to veto $\mu^+\mu^-$.

The polar angle requirement restricts tracks to the solid angle region that is well covered by the MDC. The BSC (MUID) requirement eliminates cascade events of the type $\psi' \to \pi^+\pi^- J/\psi$; followed by $J/\psi \to e^+e^-$ $(\mu^+\mu^-)$.

The surviving events are processed through a five-constraint kinematic fit to the hypothesis $\psi' \to \pi^+\pi^- p\overline{p}$. Here the highest momentum positive (negative) track is classified as the proton (antiproton).

Further cuts are made to select Δ^{++} signals.

1. Figure 19a shows the P(chi^2) distribution which pass five-constraint fit discribed above and $\chi^2_{p\overline{p}\pi^+\pi^-} < 50$. We attribute the Δ^{++} events come from
   $P(\chi^2_{p\overline{p}\pi^+\pi^-})$ <1%

2. Figure 19b shows the mass distribution of the highest momentum positive and negative tracks, there is a clear peak residing at J/ψ mass region, those events come from $\psi' \to pi^+\pi^- J/\psi$, and $J/\psi \to p\overline{p}$, we make the following cuts to get rid of those events
   $M_{p\overline{p}}$ <3.05 .or. $M_{p\overline{p}}$ >3.15 GeV/c

3. Figure 19c and d shows the mass distributions of the hypothese $p\pi^-$ and $\overline{p}\pi^+$, there are clear peaks centered at Λ and $overline\Lambda$ mass values. The cuts are made:
   $M_{\overline{p}\pi^+}$ >1.15 .or. $M_{\overline{p}\pi^+}$ <1.10 GeV/c

4. 1.112 < $M_{p\pi^+}$ < 1.352 GeV/c

5. 1.112 < $M_{\overline{p}\pi^-}$ <1.352 GeV/c

The effects of the various selection cuts on the data and the simulated event sample is summarized in Table 10.

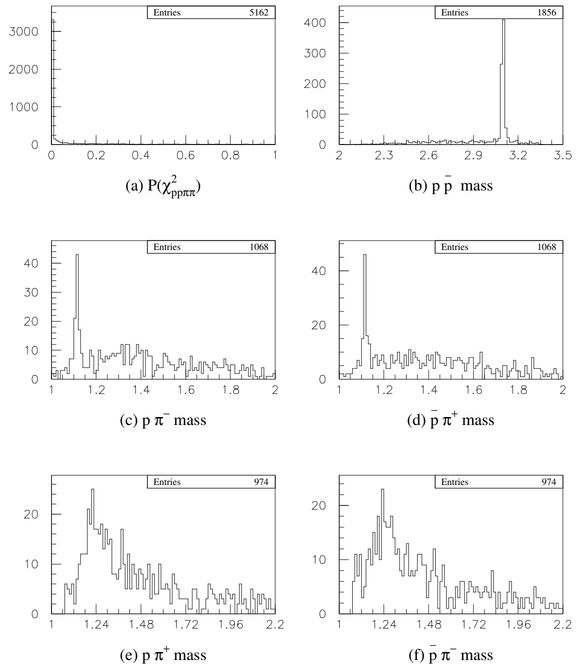

Figure 19: Plots for events that pass the selection cuts for $\psi' \to \Delta^{++}\Delta^{--}$

Table 10: A tabulation of the $\Delta^{++}\overline{\Delta}^{--}$ selection cuts.

Numbers of events surviving each requirement

	94 data	95 data	Simulated events
Preselection:	769831	1574470	
Generated			10000
skip bad runs	761640	1565447	10000
4 chrgd trks and $\sum$ q=0	317504	605583	6242
veto $\mu^+\mu^-$	310487	570412	6242
$\lvert\cos\theta_{chg}\rvert \leq 0.8$	191759	360555	4442
$\chi^2_{p\overline{p}\pi^+\pi^-} < 50.$	1802	3360	4110
Selection:			
$\mathrm{P}(\chi^2_{p\overline{p}\pi^+\pi^-}) < 1\%$	665	1191	3697
$\lvert M_{p\overline{p}} - M_{J/\psi}\rvert$ >50 MeV	368	700	3358
$\lvert M_{p\pi^-} - M_{\Lambda}$ >35 MeV	335	639	3322

4.2 Fits to the $p\pi^+$ mass distribution.

We fit the doubly charged $p\pi^+$ invariant mass distribution for the events with above cuts, shown in Fig. 20, to an p-wave Breit Wigner function with the resonance mass and width fixed at the PDG values for the Δ^{++}, of $M_0 = 1.232$ and $\Gamma_0 = 0.120$ GeV. We treat the relativistic Breit-Wigner line-shape in terms of the underlying four-body phase space, the matrix element [8] can be written as:

$$T \propto T_{prod}(m_{12}, m_{34}) P^{\Delta}(m_{12}) T^{\Delta}(m_{12}) P^{\Delta}(m_{34}) T^{\Delta}(m_{34}) \tag{1}$$

where the P^{Δ} are BW propagators, and

$$T_{prod} \propto [q_{prod}(m_{12}, m_{34})]^{L_{prod}=0}$$

$$T^{\Delta}(m_{12}) \propto [P^{\Delta}(m_{12})]^{L_{\Delta}=1}$$

$$T^{\Delta}(m_{34}) \propto [P^{\Delta}(m_{34})]^{L_{\Delta}=1}$$

$$q_{prod}(m_{12}, m_{34}) = \frac{1}{2m_{\psi'}}\sqrt{[m^2_{\psi'} - (m_{12}+m_{34})^2][m^2_{\psi'} - (m_{12}-m_{34})^2]}$$

$$L_{prod} = 0$$

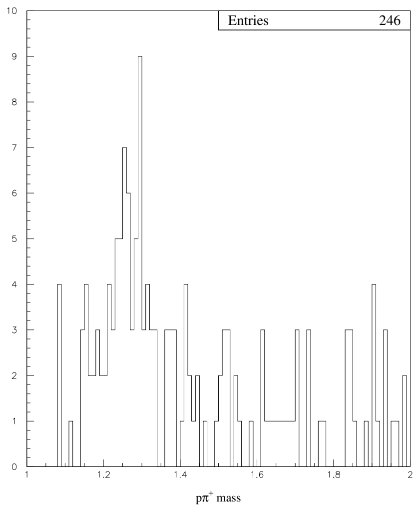

Figure 20: Fit to the invariant mass distribution of $p\pi^+$

$$q_\Delta(m) = \frac{1}{2m}\sqrt{[m^2 - (m_p + m_\pi)^2][m^2 - (m_p - m_\pi)^2]}$$

$$L_\Delta = 0$$

$$P^\Delta(m) = \frac{1}{m_\Delta^2 - m^2 - im_\Delta\Gamma_\Delta(m)}$$

where

$$\Gamma_\Delta(m) = \Gamma_\Delta^0 \cdot [\frac{q_\Delta(m)}{q_\Delta(m_\Delta)}]^{2l+1} \cdot [\frac{m_\Delta}{m}]$$

and m_Δ and Γ_Δ^0 are the PDG values.

Because the $\Gamma_\Delta(m)$ in the denominator is the total width; for the Δ^{++}, this is the same as elastic width, but in general this is not true, the Γ in the denominator should be written $\Gamma^{tot}(m) = \sum_i \Gamma^i(m)$, where the Γ^i are the partial widths, each of these has its own energy dependence.

The width is proportional to the matrix element squared integrated over the relevant phase space, not just the matrix element squared.

So, the number of events, dN, corresponding to mass intervals dm_{12} and dm_{34} is given by,

$$\frac{dN}{dm_{12}dm_{34}} \propto q_{prod}(m_{12}, m_{34}) \frac{m_{12}\Gamma^\Delta(m_{12})}{[m_\Delta^2 - m_{12}^2]^2 + m_\Delta^2[\Gamma^\Delta(m_{12})]^2} \frac{m_{34}\Gamma^\Delta(m_{34})}{[m_\Delta^2 - m_{34}^2]^2 + m_\Delta^2[\Gamma^\Delta(m_{34})]^2} \tag{2}$$

If 1 and 2 correspond to p and π^+, and 3 and 4 correspond to $\overline{p}$ and π^-, then by integrating m_{12} and m_{34} from low mass to high mass, we can get the number of events.

And looking at m_{12} by integrating m_{34} from m_{low} to m_{max}, then

$$\frac{dN}{dm_{12}} \propto \frac{m_{12}\Gamma^{\Delta}(m_{12})}{[m_{\Delta}^2 - m_{12}^2]^2 + m_{\Delta}^2[\Gamma^{\Delta}(m_{12})]^2} \cdot G(m_{12})$$

where

$$G(m_{12}) = \int_{m_{low}}^{m_{max}(m_{12})} dm_{34} \cdot \frac{q_{prod}(m_{12}, m_{34}) m_{34} \Gamma^{\Delta}(m_{34})}{[m_{\Delta}^2 - m_{34}^2]^2 + m_{\Delta}^2[\Gamma^{\Delta}(m_{34})]^2}$$

where $m_{max}(m_{12}) = min[m_{high}, m_{\psi'} - m_{12}]$

4.2.1 $\Delta^{++}\overline{\Delta}^{--}$ Background

The decay $\psi' \to \Delta^{++}\overline{\Delta}^{--}$ arises out of from $\psi' \to p\overline{p}\pi^+\pi^-$, the potential background contributions are from nonresonant population, $p\pi^+$ pair as a Δ^{++}, $p\overline{p}\pi^+\pi^-\gamma(\pi^0)$. To estimate the residual background in the sample of $\Delta^{++}\overline{\Delta}^{--}$ event candidates, we add to the resonance Breit Wigner a smooth curve of the form

$$\begin{aligned} f_{bkg}(Q) &= p_1(Q^{\frac{1}{2}} + p_2 Q^{3/2} + p_3 Q^{5/2}) \quad Q > 0 \\ &= 0 \qquad\qquad\qquad\qquad\qquad\quad Q \leq 0, \end{aligned} \tag{3}$$

The invariant mass distribution of $\psi' \to \Delta^{++}\overline{p}\pi^-$ is shown in Fig. 21.

Figure 21: Fit to the invariant mass distribution of $p\pi^+$

Table 11: A tabulation of the momenta of Σ^*

Momenta of p and π in GeV/c

	orphan π	Λ	p	decay π
max momentum	0.5	1.27	1.23	0.35
min momentum	0.0	0.72	0.49	0.0

4.3 $\psi' \rightarrow \Sigma^-(1385)\overline{\Sigma}^+(1385)$ + c.c.

The $\Sigma^\pm$ and $\Sigma^\mp$ hyperons from $\psi' \rightarrow \Sigma^\pm\overline{\Sigma}^\mp$ decays via $\Sigma^\pm \rightarrow \pi^\pm\Lambda$. We consider only those decays where the Λ's decay via the charged πp modes. The experimental signature is $\psi' \rightarrow \pi^+\pi^-\pi^+\pi^- p\overline{p}$ where one each of the $\pi^- p$ and $\pi^+\overline{p}$ combinations originate from Λ hyperons and have well separated decay vertices with a mean decay length of 7.8 cm. Not as in the case for $\psi' \rightarrow \Lambda\overline{\Lambda}$ and $\Sigma\overline{\Sigma}$, the proton (antiproton) is not always the highest momentum positive (negative) track in the final state, refering to Table 11, we did 36 different combinations for 8-constrained kinematic fit to pick up the best χ^2.

4.3.1 $\psi' \rightarrow \Sigma^-(1385)\overline{\Sigma}^+(1385)$ + c.c. Selection Criteria

We extract $\psi' \rightarrow \Sigma^-(1385)\overline{\Sigma}^+(1385)$ + c.c. event candidates using the following selection criteria:

1. six, and only six, well reconstructed charged tracks with a zero net charge and all in the polar angle region $|\cos\theta| \leq 0.8$;

2. We loop over each event 36 times, processing each possible $\pi^- p$ and $\pi^+\overline{p}$ combination through a displaced vertex-finding algorithm and then subjecting the event to a six-constraint kinematic fit to the hypothesis $\psi' \rightarrow \pi^+\pi^-\pi^+\pi^- p\overline{p}$, with the beam constraint $M_{\pi^- p} = M_{\pi^+\overline{p}} = M_\Lambda$. The combination with the best χ^2 value is selected. Telesis returns events that have $\chi^2 < 50$. The confidence level distribution for χ^2 is shown in Figure 22a.

Further cuts are made to select the Σ^* signals as follows:

1. From Figure 22a, we select the events with $P(\chi^2) < 1\%$

2. The mass recoiling against the orphan $\pi^+\pi^-$ pair, shown in Figure 22b, is dominated by a peak at the J/ψ mass (3.1 GeV), indicating lots of $\psi' \to \pi^+\pi^-\ J/\psi$; $J/\psi \to \Lambda\overline{\Lambda}$. We cut out events with $\pi^+\pi^-$ recoil mass within $\pm$ 30 MeV of the J/ψ.

3. Figure 22c and d show the $p\pi^-$ and $\overline{p}\pi^+$ mass distributions before six-constraint kinematic fit, respectively, all events which pass the above cuts are within $\pm$ 20 MeV of Λ mass region.
   $|M_{p\pi^-} - M_\Lambda| < 20$ MeV
   $|M_{\overline{p}\pi^+} - M_\Lambda| < 20$ MeV

4. The $c\tau$ distributions for the Λ and $\overline{\Lambda}$ in the remaining 33 events (2 entries/event), shown in Fig. 22e and f, has no evidence for a prompt peak at $c\tau = 0.0$.

5. Figure 23a shows the $\Lambda\pi^-$ mass distribution that recoils from a $\overline{\Lambda}\pi^+$ that are within $\pm$ 20 MeV of the $\overline{\Xi}^+$ (1.325 GeV). Twelve events appear in the Ξ^- peak. These come from $psi' \to \Xi^-\Xi^+$.

6. Figure 23b shows the mass distribution for $\Lambda\pi^-$ combinations that recoil against a $\overline{\Lambda}\pi^+$ combination within $\pm$ 50 MeV of the $\Sigma(1385)$, plus the charge conjugate. The events cluster near 1.385, indicating $\Sigma(1385)$ $\overline{\Sigma}(1385)$ decays.

The effects of the various selection cuts on the data and the simulated event sample is summarized in Table 12.

4.3.2 $\Sigma^-(1385)\overline{\Sigma}^+(1385)$ +c.c. Signal

The distribution of fitted invariant $\pi\pi p$ masses for events with $\chi^2 \leq 15$, shown in Fig. 24, has a clear and distinct peak at the $M = 1.385$ GeV Σ^- mass. We select the events within $\pm$50 MeV of the $\Sigma^\pm(1385)$ mass as $\psi' \to \Sigma^-\overline{\Sigma}^+$ plus the charge conjugate event candidates; no further cuts are made. The events cluster near 1.385, indicating $\Sigma^\pm(1385)$ $\overline{\Sigma}^\mp(1385)$ decays.

Figure 24 shows a fit of the distribution to a Breit Wigner with a phase space background and the threshold. The fit gives:

$$N_{\text{evnt}} = 15 \pm 6 \text{ events}$$

and a peak (1.396 $\pm$ 0.005) and FWHM (0.024 $\pm$ 0.013) reasonably(?) close to the ($\Sigma^+(1385)$ and $\overline{\Sigma}^-(1385)$ average) PDG values of 1.385 and 0.037, respectively.

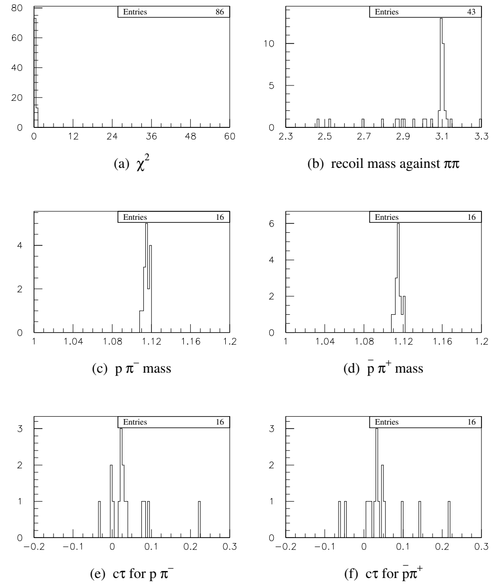

Figure 22: Distributions of events that pass criteria cuts for $\psi' \to \Sigma^-(1385)\overline{\Sigma}^+(1385)$

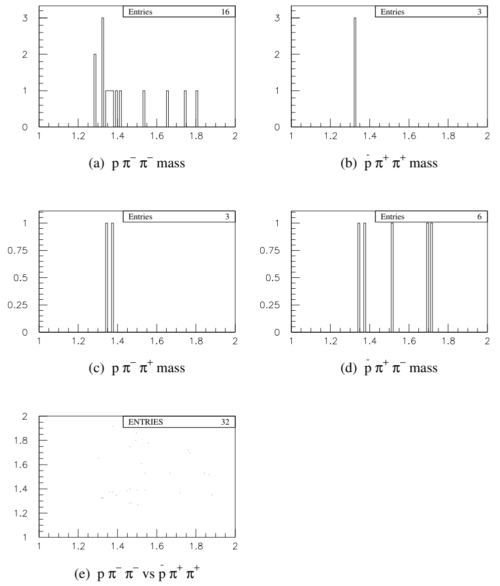

Figure 23: Mass distributions of events that pass criteria cuts for $\psi' \to \Sigma^-(1385)\overline{\Sigma}^+(1385)$

Table 12: A tabulation of the $\Sigma^-(1385)\overline{\Sigma}^+(1385)$ selection cuts.

Numbers of events surviving each requirement

	94 data	95 data	Simulated events
Preselection:	655502	1238869	
Generated			10000
skip bad runs	649193	1232381	10000
6 chrgd trks, $\sum q = 0$	335918	625466	3857
$\|\cos\theta_{chg}\| \leq 0.8$	176054	324671	2439
$\chi^2_{p\overline{p}\pi^+\pi^-} < 50.$	84	143	1578
$P(\chi^2_{p\overline{p}\pi^+\pi^-\pi^+\pi^-}) > 1\%$	45	74	1313
$\|M_{\mathrm{recoil}} - M_{J/psi}\|$ >0.03 GeV	20	28	1166
$\|M_{p\pi^-} - M_\Lambda\|$ <0.02 GeV, $\|M_{\overline{p}\pi^+} - M_\Lambda\|$ <0.02 GeV	20	26	1137
$\|M_{p\pi^-\pi^-} - M_{\Sigma^*}\|$ <0.05 GeV	4	5	985

Figure 24: A fit of the $\Lambda\pi$ distribution to a Breit Wigner with a phase space background

4.3.3 $\Sigma^-(1385)\overline{\Sigma}^+1385$ residual background

To estimate the residual background in the sample of $\Sigma^-\overline{\Sigma}^+$ + c.c. event candidates, we add to the resonance Breit Wigner a smooth curve of the form

$$\begin{aligned} f_{bkg}(Q) &= p_1(Q^{\frac{1}{2}} + p_2Q^{3/2} + p_3Q^{5/2}) \quad Q > 0 \\ &= 0 \qquad\qquad\qquad\qquad\qquad\quad Q \leq 0, \end{aligned}$$

We fit the $\Lambda\pi^\pm$ mass distribution shown in Fig. 24 to a p-wave Breit Wigner function with the resonance mass and width fixed at the PDG values for the Σ of $M_0 = 1.385$ and $\Gamma_0 = 0.036$ GeV. We fit the background under this peak.

4.4 $\psi' \to \Xi^0(1530)\overline{\Xi}^0(1530)$

We find no events and determine a 90% confidence upper limit of $Br(\psi' \to \Xi^{*0}\overline{\Xi}^{*0}) < 6.0 \times 10^{-5}$.

4.4.1 Data selection

The dominant Ξ^{*0} decay chain is

$$\begin{array}{llllll} \Xi^{*0} & \to & \Xi^-\pi^+ & & & Br = 0.67 \\ & & \Xi^- & \to & \Lambda\pi^- & Br = 1.0 \\ & & & & \Lambda \to p\pi^- & Br = 0.641, \end{array}$$

with a total branching fraction of 43% [6]. We look for $\psi' \to \Xi^{*0}\overline{\Xi^{*0}}$ events in events with the topology $\psi' \to p\overline{p}3(\pi^+\pi^-)$, i.e. eight charged tracks where a $p\pi^-$ and a $\overline{p}\pi^+$ are consistent with being from the decay of a Λ ($\overline{\Lambda}$). The proton's momenta range from 0.28 to 1.06 GeV; the pion's momenta range from 0 to 0.34 GeV.

We select events with eight charged tracks in the polar angle region $\mid \cos\theta \mid \leq 0.8$ and with zero net charge. We consider the highest momentum positive (negative) track is considered to be a proton (antiproton) and the other six tracks as pions. The tracks are subjected to 6-constraint kinematic fits to the $\psi' \to \Lambda\overline{\Lambda}\pi^+\pi^-\pi^+\pi^-$ hypothesis. The fit is applied for each of the nine possible $\Lambda \to p\pi^-$ and $\overline{\Lambda} \to \overline{p}\pi^+$ combinations for which the the $p\pi$ masses returned by the KLAMSLOW vertexing program are both within 0.05 GeV of M_Λ. Only the assignment with the best χ^2 is considered. A loose requirement of $\chi^2 < 50$ is applied.

Figure 25a (b) shows the $\Lambda\pi^-$ ($\overline{\Lambda}\pi^+$) mass distribution for the selected events. There are two entries per event. The Ξ^- shows up as a peak near 1.32 GeV and at higher masses there is some indication of the $\Sigma^*(1380)$. Figure 25c (d) shows the $\Xi^-\pi^+$ ($\overline{\Xi}^+\pi^-$) mass distribution for events with a $\Lambda\pi^-$ ($\overline{\Lambda}\pi^+$) mass within 0.025 GeV of the Ξ^-. There is no evidence for a $\Xi(1530)$ signal. Figure 25e (f) shows a scatterplot (Legoplot) of $M(\Xi^-\pi^+)$ vs $M(\overline{\Xi}^+\pi^-)$. There are no entries within 0.05 GeV of the expected position for $\psi' \to \Xi^0(1530)\overline{Xi}^0(1530)$.

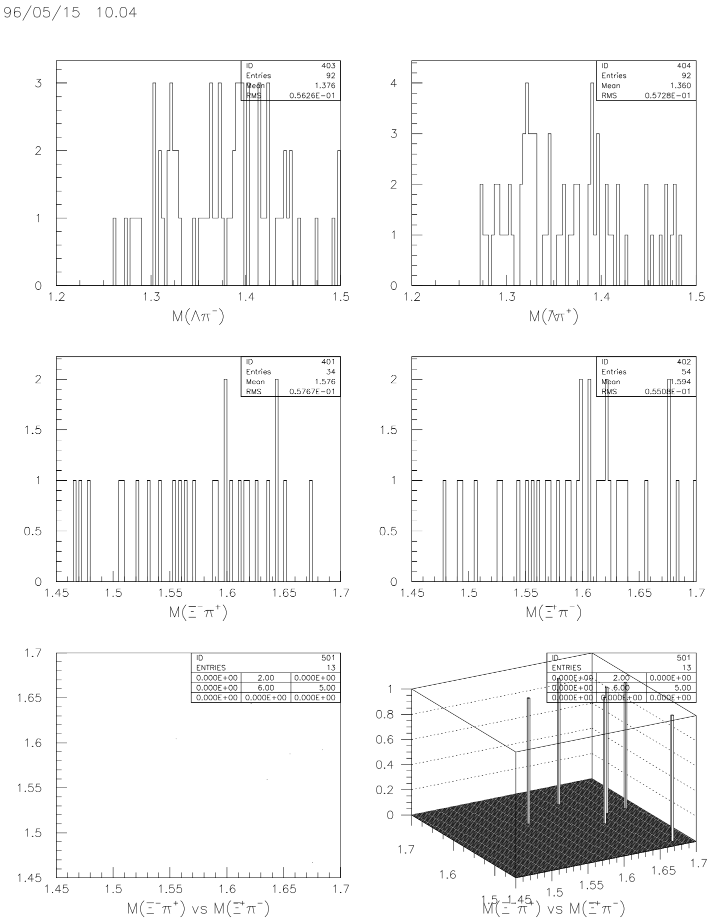

Figure 25: The **a)** $\Lambda\pi^-$, **b)** $\overline{\Lambda}\pi^+$ $\Lambda\pi^-$ ($\overline{\Lambda}\pi^+$), **c)** $\Xi^-\pi^+$ and **d)** $\overline{\Xi}^+\pi^-$ mass distributions for selected events. **e)** A scatterplot (**f**) Lego plot) of $M(\Xi^-\pi^+)$ vs $M(\overline{\Xi}^+\pi^-)$.

Figures 26a through f show the corresponding distributions for the Monte Carlo simulated events that survive the same analysis and selection procedures as are applied to the data. From a sample of 2000 generated events, 120 events survive the selections and occur within 0.05 GeV of the expected position for $\psi' \to \Xi^0(1503)\overline{Xi}^0(1530)$, corresponding to an acceptance of $\eta = 0.060 \pm 0.006$.

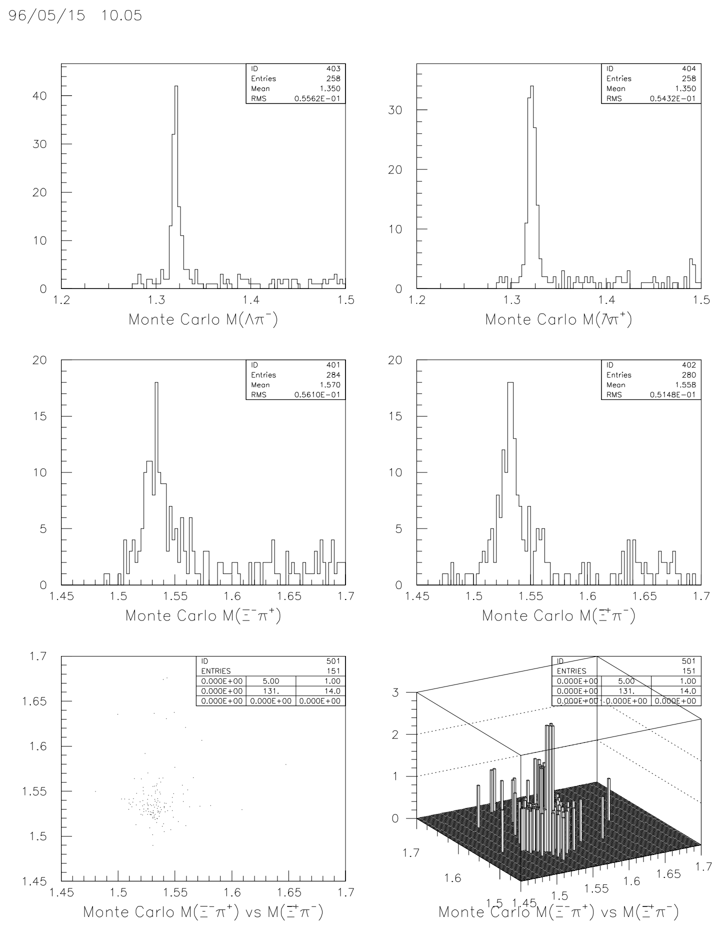

Figure 26: The Monte Carlo **a)** $\Lambda\pi^-$, **b)** $\overline{\Lambda}\pi^+$ $\Lambda\pi^-$ ($\overline{\Lambda}\pi^+$), **c)** $\Xi^-\pi^+$ and **d)** $\overline{\Xi}^+\pi^-$ mass distributions for selected events. **e)** A scatterplot (**f)** Lego plot) of $M(\Xi^-\pi^+)$ vs $M(\overline{\Xi}^+\pi^-)$ for the selected Monte Carlo events.

Table 13: A tabulation of the $\Xi(1530)\overline{\Xi}(1530)$ selection cuts.

Numbers of events surviving each requirement

	94 data	95 data	Simulated events
Generated			2000
8 chrgd trks	99383	186644	439
$\sum q = 0$	64129	118982	380
$\lvert\cos\theta\rvert \leq 0.8$	24935	45406	213
$\chi^2_{8c} \leq 50$	16	30	129

The effects of the various selection cuts on the data and the simulated event sample is summarized in Table 13.

4.4.2 Results

We determine the 90% confidence level upper limit for the $\psi' \to \Xi^0(1530)\overline{\Xi}^0(1530)$ branching ratio from the relation

$$Br[\psi' \to \Xi^0(1530)\overline{\Xi}^0(1530)] < \frac{N^{limit}_{evts}}{N_{\psi'}\eta\ Br(\Xi^0(1530) \to \Xi^-\pi^+)^2 Br(\Lambda \to p\pi^-)^2}, \quad (4)$$

where $N^{limit}_{evts} = 2.3$, $N_{\psi'} = (3.44 \pm 0.31) \times 10^6$ is the number of $\psi's$ in the events sample [?], $\eta = 0.06$ is the detection efficiency and the branching ratios $Br(\Xi^0(1530) \to \Xi^-\pi^+) = 0.67$ and $Br(\Lambda \to p\pi^-) = 0.641 \pm 0.005$ are taken from the PDG tables [6]. The result is

$$Br[\psi' \to \Xi^0(1530)\overline{\Xi}^0(1530)] < 6.0 \times 10^{-5}. \quad (5)$$

This mode is accessible for J/ψ decays it is just barely energetically possible. There are no entries for it in the PDG avaiable for comparison.

4.5 $\psi' \to \Omega^-\overline{\Omega}^+$

We find no events and determine a 90% confidence upper limit of $Br(\psi' \to \Omega^-\overline{\Omega}^+) < 1.0 \times 10^{-4}$.

Table 14: A tabulation of the momenta of Ω production

Momenta of Ω production in GeV/c

	π	Λ	p	k
max momentum	0.238	0.76	0.76	0.48
min momentum	0.0	0.29	0.14	0.02

4.5.1 Data selection

The dominant Ω^- decay chain is

$$\begin{array}{llllll} \Omega^- & \rightarrow & \Lambda K^- & & & Br = 0.678 \\ & & \Lambda & \rightarrow & p\pi^- & Br = 0.641, \end{array}$$

with a total branching fraction of 43% [6]. We look for $\psi' \rightarrow \Omega^- \overline{\Omega}^+$ events in events with the topology $\psi' \rightarrow p\overline{p}\pi^+\pi^- K^+ K^-$, i.e. six charged tracks where the $p\pi^-$ and a $\overline{p}\pi^+$ are consistent with being from the decay of a Λ ($\overline{\Lambda}$). The proton's momenta range from 0.14 to 0.76 GeV; the pion's momenta range from 0 to 0.24 GeV, and the kaon's momenta range from 0.02 to 0.481 GeV, see details in the Table 14.

We select events with six charged tracks in the polar angle region $\mid \cos\theta \mid \leq 0.8$ and with zero net charge. We reject events where *both* the highest momentum positive and negative tracks are identified as being both muons or both electrons. The is subjected to a 7-constraint kinematic fits to the $\psi' \rightarrow \Lambda\overline{\Lambda}K^+K^-$ hypothesis, with the ΛK^- invariant mass is constrained to equal that of the $\overline{\Lambda}K^+$. The fit is applied for each of the 36 particle assignment possibilities. Only the assignment with the best χ^2 is considered. A loose requirement of $\chi^2 < 50$ is applied. The exact same analysis was applied to a sample of 2000 Monte Carlo simulated events.

Figure 27a shows the ΛK^- mass distribution for the selected events. Figure 27b shows the same distribution for the selected Monte Carlo events. In the Monte Carlo event sample, the Ω^- shows up as a peak of 71 events near 1.672 GeV; all of the events are within 0.01 GeV of the nominal Ω^- mass of 1.672 GeV, which was used in the generator. There are no events in the data sample closer than 0.02 GeV to the nominal Ω^- mass.

The effects of the various selection cuts on the data and the simulated event sample are summarized in Table 15.

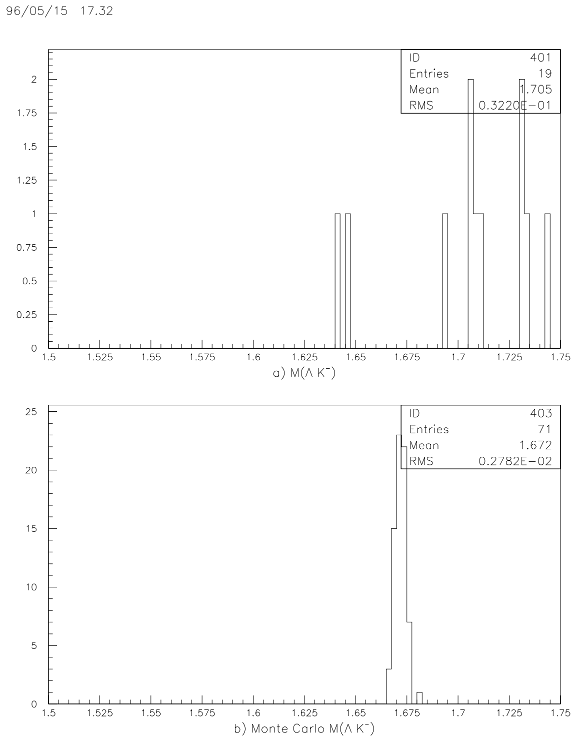

Figure 27: **a)** The ΛK^- invariant mass for the selected events from the data sample. **a)** The same distribution for the Monte Carlo event sample.

Table 15: A tabulation of the $\Omega^-\overline{\Omega}^+$ selection cuts.

Numbers of events surviving each requirement

	94 data	95 data	Simulated events
Generated			2000
8 chrgd trks			505
$\sum q = 0$	334618	619912	437
less than 2 μ's	334152	618162	437
less than 2 μ's	333854	617600	437
$\lvert\cos\theta\rvert \leq 0.8$	178092	326922	264
2 good Λ's	28759	53379	205
$\chi^2_{8c} \leq 50$	8	11	71

4.5.2 Results

We determine the 90% confidence level upper limit for the $\psi' \to \Omega^-\overline{\Omega}^+$ branching ratio from the relation

$$Br(\psi' \to \Omega^-\overline{\Omega}^+) < \frac{N_{evts}^{limit}}{N_{\psi'}\eta\ Br(\Omega^- \to \Lambda K^-)^2 Br(\Lambda \to p\pi^-)^2}, \tag{6}$$

where $N_{evts}^{limit} = 2.3$, $N_{\psi'} = (3.44 \pm 0.31) \times 10^6$ is the number of $\psi's$ in the events sample [?], $\eta = 0.035$ is the detection efficiency and the branching ratios $Br(\Omega^- \to \Lambda K^-) = 0.678 \pm 0.007$ and $Br(\Lambda \to p\pi^-) = 0.641 \pm 0.005$ are taken from the PDG tables [6]. The result is

$$Br(\psi' \to \Omega^-\overline{\Omega}^+) < 1.0 \times 10^{-4}. \tag{7}$$

This mode is energetically inaccessible for J/ψ decays.

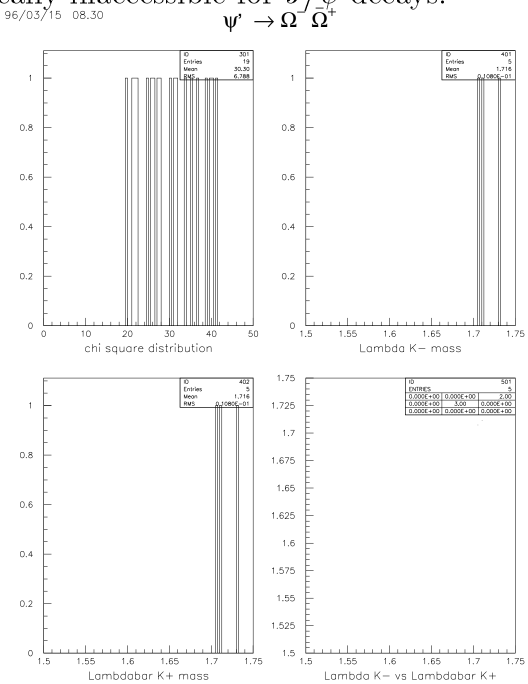

Figure 28: Distributions of events that pass the cuts for $\psi' \to \Omega^-\overline{\Omega}^+$

4.6 Acceptance and Efficiency of the Decuplet Pairs

We determine the acceptance for the decuplet hyperon-pair channels completely from Monte Carlo simulated events. Here we generated events with a uniform $\cos\theta$ distribution, determined the acceptance for the various event selection criteria and then corrected it analytically to $\alpha = 0.6$ and included the change in the acceptance as a systematic error for $\Delta^{++}\overline{\Delta}^{--}$ and $\Sigma^{-}\overline{\Sigma}^{+} + cc$. The resulting acceptances are as follows:

Decay Mode	acceptance
$\Delta^{++}\overline{\Delta}^{--}$	0.24 ± 0.02
$\Delta^{++}\overline{P}\pi^{-}$	0.24 ± 0.015
$\Sigma^{-}\overline{\Sigma}^{+} + cc$	0.11 ± 0.01
$\Xi^{0}\overline{\Xi}^{0}$	0.05
$\Omega^{-}\overline{\Omega}^{+}$	0.05

In the hyperon modes we require two Λ's that decay to charged $p\pi$ final states, which has a branching fraction $Br(\Lambda \to p\pi^{-}) = 0.639 \pm 0.005$; $Br(\Sigma^{*} \to \Lambda\pi) = 0.88 \pm 0.002$; the other decay modes that are required are very nearly unity, namely $Br(\Xi^{0} \to \Xi^{-}\pi^{+}) = 1.0$ and $Br(\Xi^{-} \to \Lambda\pi^{-}) = 0.999$ [6]. The efficiency for each channel is the $\Lambda \to p\pi^{-}$ branching fraction squared: 0.408 ± 0.006.

5 Continuum background

A few percent of the hadronic events in our data sample originate from non-resonant $e^{+}e^{-} \to q\overline{q}$ annihilation events. We use a 22.7 pb^{-1} data sample taken off resonance at $\sqrt{s} = 4.03$ GeV to limit the level of continuum $e^{+}e^{-} \to B_{8}\overline{B_{8}}$ contamination to our event samples. We find no events that survive the analysis procedures and event selection criteria identical described above for the $\Lambda\overline{\Lambda}$ mode. Neither is there any evidence for a $p\overline{p}$ signal: there are four events that satisfy the $p\overline{p}$ selection criteria including the $\chi^{2}_{p\overline{p}} < 15$ requirement, but these are the tail of a much larger number of high χ^{2} events.

Although the off-resonance running is at a higher cm energy than the ψ' resonance, and the $e^{+}e^{-} \to B_{8}\overline{B_{8}}$ cross section is expected to be smaller, the integrated luminosity that is sampled is considerably higher (by almost a factor of four). We conclude that continuum events comprise a negligibly small contamination to our data samples.

6 Determination of the total number of ψ' events

We determine the number of ψ' events in our data samples from the observed number of cascade decays of the type $\psi' \to \pi^{+}\pi^{-}J/\psi$; $J/\psi \to \mu^{+}\mu^{-}$. For these, we require:

1. four, and only four, charged tracks with zero net charge;

2. the highest momentum positive and negative tracks tracks are in the polar angle region $|\cos\theta| \leq 0.6$; the other tracks are in the region $|\cos\theta| \leq 0.8$; and

3. at least one of the high momentum tracks is positively identified as a muon.

The polar angle requirement on the high momentum tracks ensures that these tracks are well within the solid-angle acceptance of the MUID system.

These events, with no further selections, are subjected to a four-constraint kinematic fit to the hypothesis $\psi' \to \pi^+\pi^-\mu^+\mu^-$. The distribution of $\mu^+\mu^-$ masses for the events that pass the fit, shown in Fig. 29, is dominated by a peak at the J/ψ mass. Events with $3.05 < M_{\mu\mu} < 3.15$ GeV are selected as $\psi' \to \pi^+\pi^- J/\psi$; $J/\psi \to \mu^+\mu^-$ event candidates. This is a very clean event sample with negligible background.

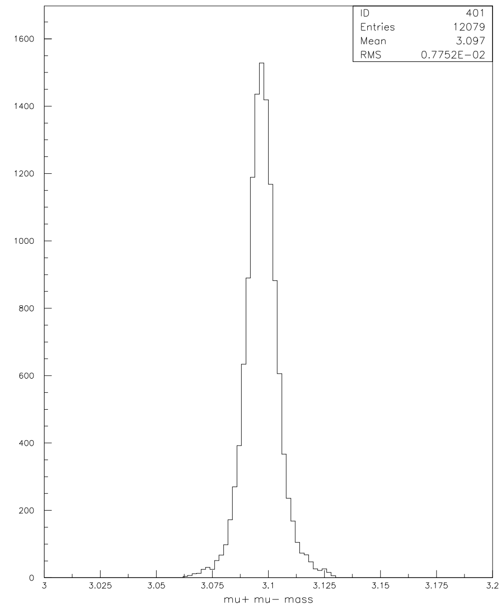

Figure 29: The fitted $M_{\mu\mu}$ distribution for events with at least one identified muon that fit to $\psi' \to \pi^+\pi^-\mu^+\mu^-$.

We determine the total number of ψ's in the data sample from the relation

$$N_{\psi'} = \frac{N_0}{\epsilon Br(\psi' \to \pi^+\pi^- J/\psi) Br(J/\psi \to \mu^+\mu^-)},$$

where N_0 is the number of events under the J/ψ peak in Fig. 29, ϵ is the combined acceptance and efficiency, and $Br(\psi' \to \pi^+\pi^- J/\psi) = 0.324 \pm 0.026$ and $Br(J/\psi \to$

$\mu^+\mu^-) = 0.060 \pm 0.003$ are taken from the PDG tables [6]. The acceptance/efficiency, $\epsilon = 0.24 \pm 0.01$ is determined from a sample of Monte Carlo simulated events that are subjected to the same event selection criteria as are used for the data.

The total number of ψ' events in the four-track data sample is determined to be

$$N_{\psi'} = 3.44 \pm 0.31 \times 10^6,$$

where the error is dominated by the error on the $\psi' \to \pi^+\pi^- J/\psi$ branching fraction. Because of the occasional presence of additional *"ghost"* tracks, mostly due to multiple counting of real tracks, the four and only four track requirement imposes a small ($\simeq$ 3%) event loss. Since a similar event loss is expected in the $\psi' \to B_i\overline{B_i}$ event samples described above, we apply no correction for this effect and assume that it cancels out in the branching fraction calculations described below.

7 Acceptance and efficiency

7.1 $p\overline{p}$:

acceptance: We determine the acceptance for $\psi' \to p\overline{p}$ events from a sample of Monte Carlo simulated events. These events were generated with an angular distribution that is flat in $\cos\theta$. This angular distribution has been measured for $J/\psi \to p\overline{p}$ decays where a

$$\frac{dN}{d\cos\theta} \propto 1 + \alpha\cos^2\theta$$

dependence is seen with $\alpha = 0.61 \pm 0.23$ for [7].

Of 10,000 simulated events, 5,753 pass the solid angle, momentum difference and chi-squared cuts. We analytically adjust the acceptance implied by this number to a value of $\alpha = 0.6$ and increase the error in the acceptance to account for changes resulting from varying α by one $\pm$ standard deviation from its J/ψ value. The resulting acceptance value is 0.52 ± 0.03.

efficiency: We determine the efficiency of the TOF, BSC, and unmatched BSC energy cuts using a sample of $\psi' \to \pi^+\pi^- J/\psi$; $J/\psi \to p\overline{p}$ events. These events, selected by MDC information alone, provide a very clean sample of nearly back-to-back $p\overline{p}$ pairs with kinematics similar to those from $\psi' \to p\overline{p}$. With these events we determine and efficiency for our $p\overline{p}$ event selection of 0.63 ± 0.04.

7.2 $\Lambda\overline{\Lambda}$, $\Sigma^0\overline{\Sigma}^0$, and $\Xi^-\overline{\Xi}^+$:

acceptance: We determine the acceptance for the hyperon-pair channels completely from Monte Carlo simulated events. Here we generated events with a uniform $\cos\theta$ distribution, determined the acceptance for the various event selection criteria and then corrected it analytically to $\alpha = 0.6$ and included the change in the acceptance as a systematic error. The resulting acceptances are as follows:

Decay Mode	acceptance
$\Lambda\overline{\Lambda}$	0.24 ± 0.02
$\Sigma^0\overline{\Sigma}^0$	0.074 ± 0.015
$\Xi^-\overline{\Xi}^+$	0.11 ± 0.01

Here the error on the $\Sigma^0\overline{\Sigma}^0$ acceptance is increased to reflect uncertainties in the the Monte Carlo simulation of low energy photons.

efficiency: In the three hyperon modes we require two Λ's that decay to charged $p\pi$ final states, which has a branching fraction $Br(\Lambda \to p\pi^-) = 0.639 \pm 0.005$; the other decay modes that are required are very nearly unity, namely $Br(\Sigma \to \Lambda\gamma) = 1.0$ and $Br(\Xi^- \to \Lambda\pi^-) = 0.999$ [6]. The efficiency for each channel is the $\Lambda \to p\pi^-$ branching fraction squared: 0.408 ± 0.006.

8 Results

The branching fractions are determined from the expression

$$Br(\psi' \to X) = \frac{N_X - N_{bkgd}}{N_{\psi'}\epsilon},$$

where N_X, N_{bkgd}, $N_{\psi'}$, and ϵ are the numbers of selected events, background events, the total number ψ's, and the combined acceptance and efficiency, respectively. The values of these quantities and the resulting branching fraction for each decay mode are listed below.

mode	N_{evt}	N_{bkg}	acceptance	efficiency	Br $(\times 10^{-4})$
$p\overline{p}$	320 ± 18	14 ± 14	0.52 ± 0.03	0.63 ± 0.04	$2.73 \pm 0.21 \pm 0.33$
$\Lambda\overline{\Lambda}$	77 ± 8.8	5 ± 5	0.24 ± 0.02	0.41 ± 0.01	$2.14 \pm 0.31 \pm 0.26$
$\Sigma^0\overline{\Sigma}^0$	10.9 ± 3.7	*	0.074 ± 0.015	0.41 ± 0.01	$1.11 \pm 0.38 \pm 0.25$
$\Xi^-\overline{\Xi}^+$	14 ± 4	1.4 ± 1.4	0.11 ± 0.01	0.41 ± 0.01	$0.83 \pm 0.28 \pm 0.12$

*(The N_{evt} entry for the Σ^0 mode is already background subtracted.)

We plot our results for the branching fractions in Fig. 1, along with previous limits and results. Our measured value for the $Br(\psi' \to p\overline{p})$ is about one standard deviation higher than the previous DASP measurements, which was based on 4 events [3] and a Mark I measurement with similar statistics [4]. The results for $\Lambda\overline{\Lambda}$ and $\Xi^-\overline{\Xi^-}$ are below the PDG upper limit values. There are no previous experimental results for $\Sigma^0\overline{\Sigma^0}$.

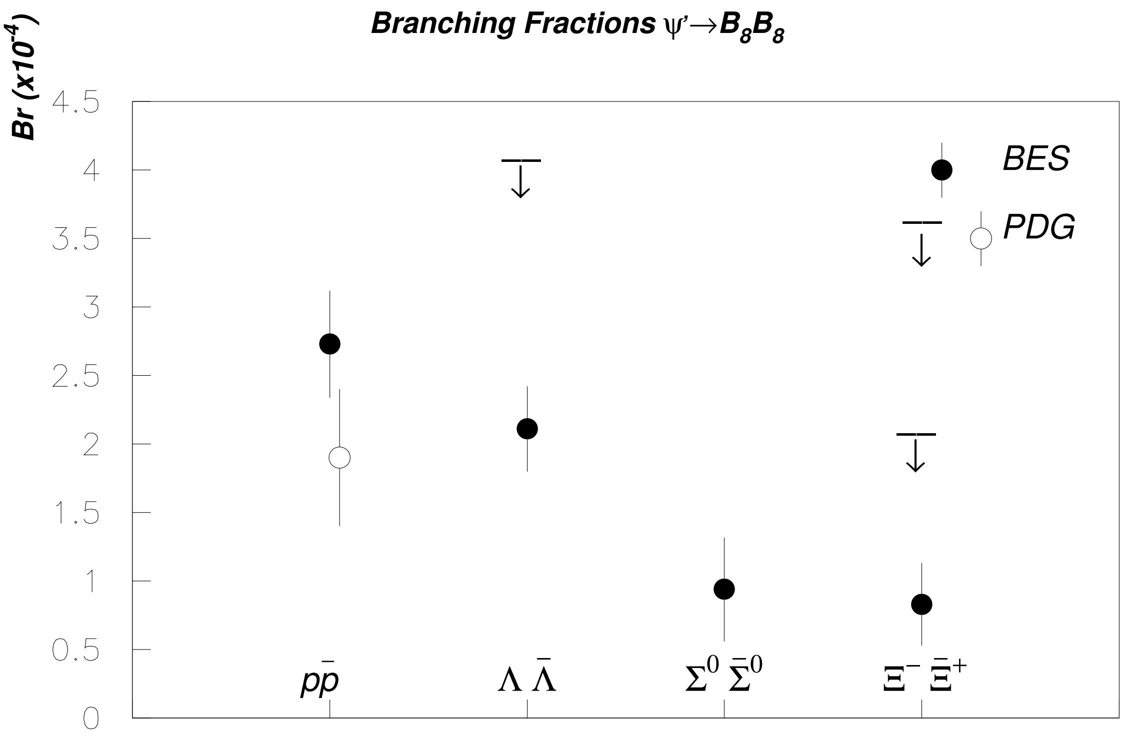

Figure 30: The measured branching fractions for $\psi' \to B_i\overline{B_i}$ decays, $B_i = p,\ \Lambda,\ \Sigma^0$ and Ξ^-. Previous measurements are indicated for comparison.

In Fig. 31, we plot the reduced branching fractions derived from our measurements. The results show a trend to smaller values for the higher massses, similar to that seen for the J/ψ (shown above in Fig. 1), and is only marginally consistent with expectations from flavor-$SU(3)$ symmetry. Higher precision measurements *both* for the J/ψ and ψ' would clarify this issue.

Our measured ψ' branching fractions agree with expectations derived from the application of the 14% rule to the PDG values for the corresponding J/ψ decays:

Decay Mode			Br	0.147×Br
J/ψ	$\rightarrow$	$p\overline{p}$	$(2.14 \pm 0.10) \times 10^{-3}$	$(3.15 \pm 0.15) \times 10^{-4}$
	$\rightarrow$	$\Lambda\overline{\Lambda}$	$(1.35 \pm 0.14) \times 10^{-3}$	$(1.98 \pm 0.21) \times 10^{-4}$
	$\rightarrow$	$\Sigma^0\overline{\Sigma}^0$	$(1.3 \pm 0.2) \times 10^{-3}$	$(1.9 \pm 0.3) \times 10^{-4}$
	$\rightarrow$	$\Xi^-\overline{\Xi}^+$	$(0.9 \pm 0.2) \times 10^{-3}$	$(1.3 \pm 0.3) \times 10^{-4}$.

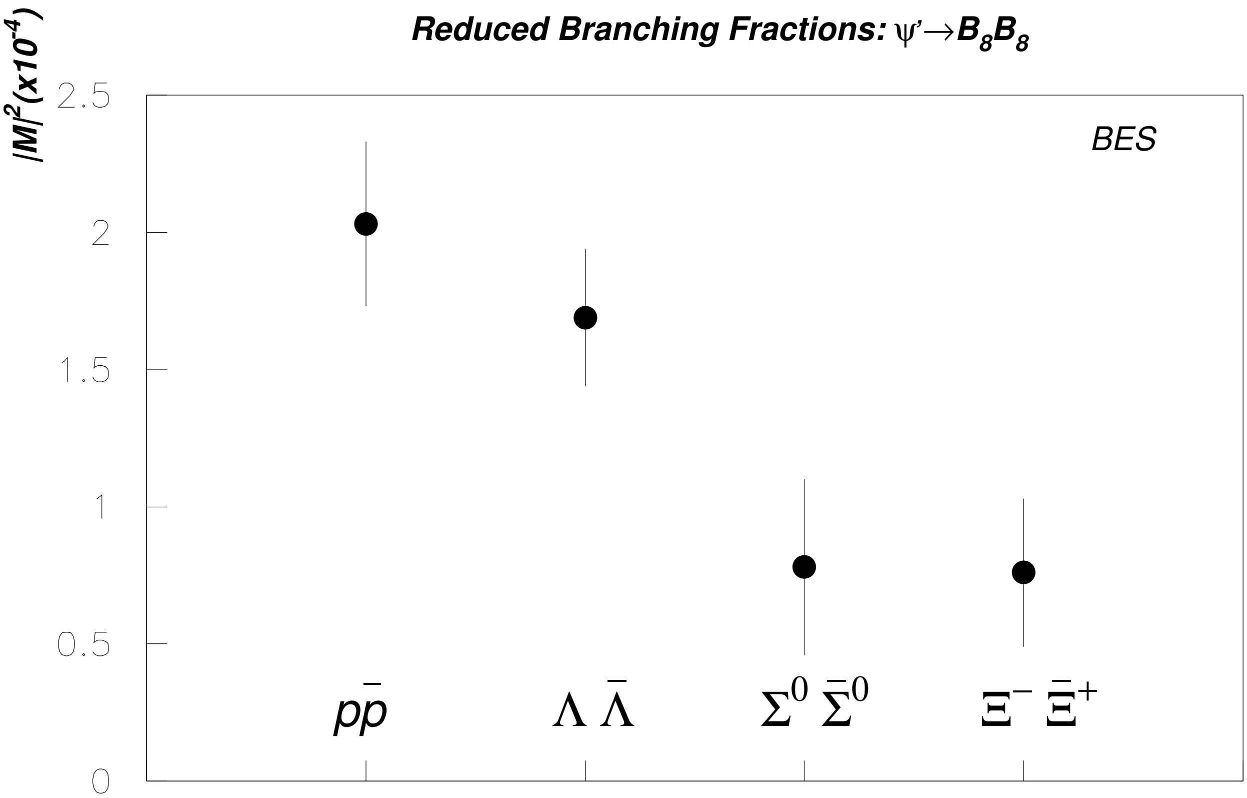

Figure 31: The reduced branching fractions $|M_i|^2$ for $\psi' \rightarrow B_i\overline{B_i}$ decays.

8.1 Results

The values of the resulting branching fraction for each decay mode are listed below.

mode	N_{evt}	acceptance	efficiency	Br ($\times 10^{-4}$)
$\Delta^{++}\overline{\Delta}^{--}$	67 ± 29	0.24 ± 0.01	1.0	0.81 ± 0.5
$\Sigma^{-}\overline{\Sigma}^{+}$+cc	14 ± 4	0.10 ± 0.01	$\pm$	$1.36 \pm 0.5 \pm 0.19$
$\Xi^{0}\overline{\Xi}^{0}$	0	0.05	0.18 ± 0.01	< 0.72
$\Omega^{-}\overline{\Omega}^{+}$	0	0.05	0.19 ± 0.01	< 0.71

The N_{evt} entries for these modes are already background subtracted. We plot our results for the branching fractions in Fig. 32, There are no previous experimental results for those modes. Currently we only give upper limits for $\Xi^0\overline{\Xi}^0$ and $\Omega^-\overline{\Omega}^+$, we need more ψ' data to study these two modes.

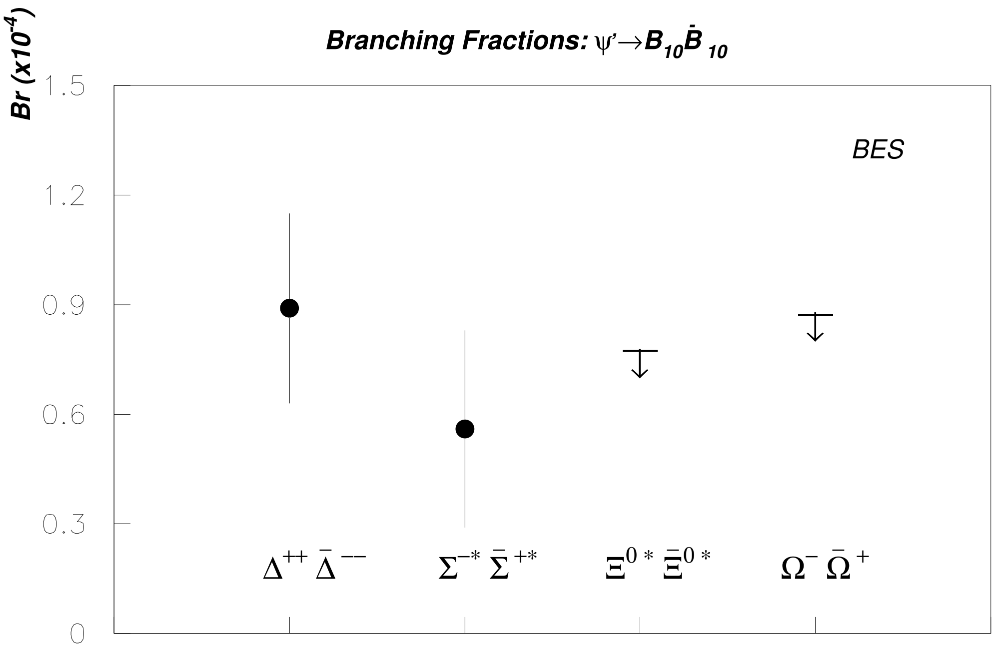

Figure 32: The measured branching fractions for $\psi' \rightarrow B_i\overline{B_i}$ decays,B_i = Δ^{++}, $\Sigma^{*\,+}$, $\Xi^{0\,*}$ and Ω^-.

In Fig. 33, we plot the reduced branching fractions derived from our measurements.

Our measured ψ' branching fractions agree with expectations derived from the application of the 14% rule to the PDG values for the corresponding J/ψ decays for $\Delta^{++}\overline{\Delta}^{--}$ and $\Sigma^-\overline{\Sigma}^+$, no entry in J/$\psi$ to $\Xi^0(1530)\overline{\Xi}^0(1530)$ and $\Omega^-\overline{\Omega}^+$.

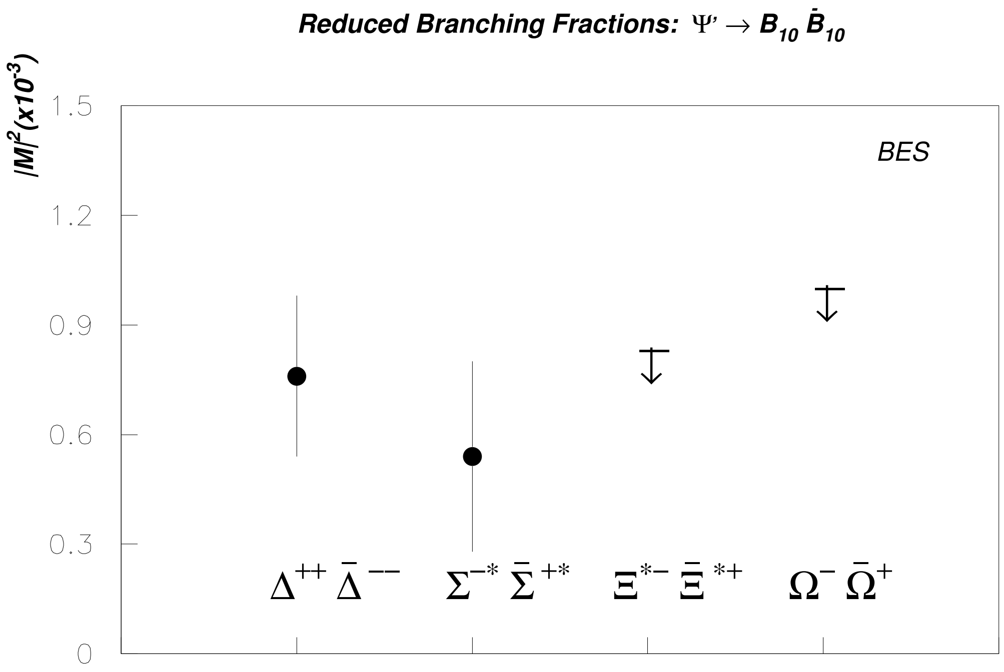

Figure 33: The reduced branching fractions $|M_i|^2$ for $\psi' \to B_i\overline{B_i}$ decuplet decays.

Decay Mode			Br	0.147×Br
J/ψ	$\rightarrow$	$\Delta^{++}\overline{\Delta}^{--}$	$(1.10 \pm 0.29) \times 10^{-3}$	$(1.62 \pm 0.5) \times 10^{-4}$
	$\rightarrow$	$\Sigma^{-}\overline{\Sigma}^{+}$ + cc	$(1.03 \pm 0.13) \times 10^{-3}$	$(1.40 \pm 0.24) \times 10^{-4}$

9 Conclusion

We report preliminary measurements of the branching fractions for $\psi' \rightarrow p\overline{p}$, $\Lambda\overline{\Lambda}$, $\Sigma^0\overline{\Sigma^0}$, and $\Xi^-\overline{\Xi^-}$. The measured branching fractions agree with expectations based on an application of the 14% rule to the corresponding J/ψ decays. The reduced branching fractions decrease with increasing baryon masses, showing some deviation from expectations based on flavor-$SU(3)$ symmetry.

10 Acknowledgements

We thank the staffs of the BEPC accelerator and the IHEP computing center for their assistance.

References

[*] Present address: Stanford Linear Accelerator Center, Stanford, California 94309.

[†] Work supported in part by the National Natural Science Foundation of China under Contract No. 19290400 and the Chinese Academy of Sciences under contract No. KJ85 (IHEP); by the Department of Energy under Contract Nos. DE-FG02-91ER40676 (Boston University), DE-FG03-92ER40701 (Caltech), DE-FG03-93ER40788 (Colorado State University), DE-AC02-76ER03069 (MIT), DE-AC03-76SF00515 (SLAC), DE-FG03-91ER40679 (UC Irvine), DE-FG03-94ER40833 (U Hawaii), DE-FG05-92ER40736 (UT Dallas), DE-AC35-89ER40486 (SSC Lab); by the U.S. National Science Foundation, Grant No. PHY9203212 (University of Washington); and by the Texas National Research Laboratory Commission under Contract Nos. RGFY91B5, RGFY92B5 (Colorado State), and RCFY93-316H (UT Dallas).

[1] M.E.B. Franklin et al. (Mark II Collaboration), Phys. Rev. Lett. **51**, 963 (1983).

[2] M. Mangano (CDF collaboration), proceedings of the XXIX Rencontres de Moriond on QCD and High Energy Hadronic Interactions, Meribel, March 1994; and the XVIIth International Conference on High Energy Physics, Glasgow, July, 1994.

[3] R. Brandelick et al. (DASP Collaboration), Z. Phys. **C1**, 233 (1979).

[4] G. Feldman and M. Perl (Mark I Collaboration), Phys. Rep. **C33**, 285 (1977).

[5] J.Z. Bai et al. (BES Collaboration), Nucl. Inst. and Meth. **A344**, 319 (1994).

[6] L. Montanet et al. (Particle Data Group), *Review of Particle Properties,* Phys. Rev. **D50**, 1173 (1994).

[7] M.W. Eaton et al. (Mark II Collaboration), Phys. Rev. **D29**, 804 (1984).

[8] W.M. Dunwoodie, private communication.